Laboratory of Biopharmaceutical Research[1], National Institute of Biomedical Innovation; Laboratory of Toxicology and Safety Science[2], Graduate School of Pharmaceutical Sciences; The Center for Advanced Medical Engineering and Informatics[3]; Laboratory of Biomedical Innovation[4], Graduate School of Pharmaceutical Sciences, Osaka University, Osaka, Japan

Rho GDP-dissociation inhibitor alpha is associated with cancer metastasis in colon and prostate cancer

T. YAMASHITA[1,2,*], T. OKAMURA[1,*], K. NAGANO[1,*], S. IMAI[1], Y. ABE[1], H. NABESHI[1,2], T. YOSHIKAWA[1,2], Y. YOSHIOKA[1,2,3], H. KAMADA[1,3], Y. TSUTSUMI[1,2,3], S. TSUNODA[1,3,4]

Received July 7, 2011, accepted August 5, 2011

Shin-ichi Tsunoda, Ph.D, Laboratory of Biopharmaceutical Research, National Institute of Biomedical Innovation, 7-6-8 Saito-Asagi, Ibaraki, Osaka 567-0085, Japan.
tsunoda@nibio.go.jp
**These authors contributed equally to the work.*

Pharmazie 67: 253–255 (2012) *doi: 10.1691/ph.2012.1630*

Since metastasis is one of the most important prognostic factors in colorectal cancer, development of new methods to diagnose and prevent metastasis is highly desirable. However, the molecular mechanisms leading to the metastatic phenotype have not been well elucidated. In this study, a proteomics-based search was carried out for metastasis-related proteins in colorectal cancer by analyzing the differential expression of proteins in primary versus metastasis focus-derived colorectal tumor cells. Protein expression profiles were determined using a tissue microarray (TMA), and the results identified Rho GDP-dissociation inhibitor alpha (Rho GDI) as a metastasis-related protein in colon and prostate cancer patients. Consequently, Rho GDI may be useful as a diagnostic biomarker and/or a therapeutic to prevent colon and prostate cancer metastasis.

1. Introduction

Colorectal cancer is known as a major metastatic cancer, and 40–50% of patients already have a metastatic focus at presentation. Moreover, the 5-year survival of these patients is under 10% (Davies et al. 2005). Thus, metastasis is one of the most important prognostic factors in colorectal cancer. In order to improve rates of cancer remission, it will be necessary to clarify the detailed molecular mechanisms of cancer metastasis and to utilize this information to establish new diagnostic and therapeutic techniques. Many researchers have searched for metastasis-related molecules (Liu et al. 2010; Shuehara et al. 2011) using proteomics techniques (Hanash 2003). Comprehensive mapping of the molecular changes during metastasis would greatly improve our understanding of the recurrence and management of cancer. However, the knowledge gained so far in these studies has not been sufficient to improve cancer remission rates.

Here we show the potential of Rho GDI as a metastasis-related protein in colon and prostate cancer patients. In order to identify metastasis-related proteins, the protein expression patterns of human colorectal cancer cells with different metastatic characters were compared. Because these cells were derived from the same patient (SW480: a surgical specimen of a primary colon adenocarcinoma, SW620: a lymph node metastatic focus), cancer metastasis-related protein candidates could be effectively sought without background variations due to differences between individuals. Furthermore, by analyzing the expression of candidate proteins in many clinical samples using a TMA, we attempted to validate the association of these candidates with metastasis. TMA is a slide glass containing many clinical tissues, and it enables one to carry out a high-throughput analysis by evaluating the relationship between expression profiles of each candidate molecule and clinical information such as metastasis. (Imai et al. 2011; Yoshida et al. 2011).

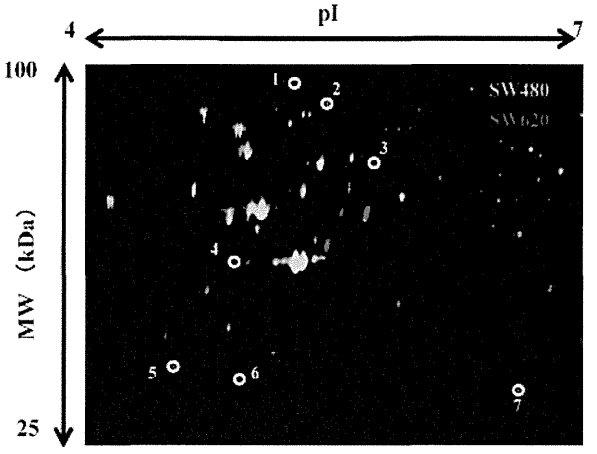

Fig. 1: 2D-DIGE image of fluorescently-labeled proteins from different metastatic human colorectal cancer cells. SW480 is human colorectal cancer cell line derived from a primary tumor and SW620 is derived from a metastatic focus from the same patient. Proteins from the colon cancer cells (SW480, SW620) were labeled with Cy3 and Cy5 respectively, and analyzed by 2D electrophoresis. The differentially-expressed spots (white circles) were then identified by LC-UHR TOF/MS

Table 1: High expression proteins in SW620 compared to SW480

	Accession	Protein name	MW (kDa)	pI	Ratio (SW620 / SW480)
1	P12109	collagen alpha-1(VI) chain	108.6	5.3	1.53
2	Q15459	splicing factor 3A subunit 1	88.9	5.2	1.61
3	P13797	T-plastin	70.9	5.5	1.59
4	P60709	actin cytoplasmic 1	42.1	5.3	1.50
5	P63104	14-3-3 zeta/delta	27.9	4.7	1.63
6	P52565	Rho GDP-dissociation inhibitor 1 (Rho GDI)	23.3	5.0	1.90
7	P30041	Peroxiredoxin-6 (PRDX6)	25.1	6.0	1.86

2. Investigations, results and discussion

In order to search for metastasis-related proteins, we analyzed differentially-expressed proteins between SW480 and SW620 by two-dimensional differential in-gel electrophoresis (2D-DIGE) (Fig. 1). As a result, 7 spots with at least a 1.5-fold-altered expression level were found by quantitative analysis, and these spots were identified by mass spectrometry (Table 1). Three molecules having a high SW620/SW480 expression ratio indicating a strong association with cancer metastasis were identified: Rho GDP-dissociation inhibitor alpha (Rho GDI), peroxiredoxin-6 (PRDX6) and 14-3-3 zeta/delta.

The expression profiles of these proteins were analyzed by immunohistochemistry using the TMA with colon cancer and multiple cancer tissues. Results of this analysis indicated that expression of PRDX6 and 14–3-3 zeta/delta had no relationship to the clinical status of cancer metastasis (data not shown). On the other hand, in positive cases of lymph node metastasis, the expression ratio of Rho GDI was significantly higher than in the negative cases. Furthermore, the same trend was seen when tissues from prostate cancer patients were analyzed (Table 2).

To confirm these results, the expression levels of Rho GDI protein in colon cancer cell lines with different metastatic potential (SW480 < SW620 < SW620-OK1 < SW620-OK2: Characteristics of SW620-OK1 and SW620-OK2 are described in *Experimental*) were investigated by western blot analysis (Fig. 2). The expression of Rho GDI was found to be up-regulated with the development of metastatic characteristics. These results suggested that Rho GDI is correlated with cancer metastasis.

Rho GDI has been identified as key regulator of Rho family GTPases. Activation of growth factor receptors and integrins can promote the exchange of GDP for GTP on Rho proteins (Bishop et al. 2000). Furthermore, GTP-bound Rho proteins interact with a range of effector molecules to modulate their activity or localization, and this leads to changes in cell behavior. It is clear that Rho family GTPases are involved in the control of cell morphology and motility (Etienne-Manneville et al. 2002; Hall et al. 1997; Van Aelst et al. 1997). The importance of Rho protein and Rho GDI in cancer progression, particularly in the area of metastasis, is becoming increasingly evident. Recently, some reports have indicated that the expression of Rho GDI was correlated with colorectal and breast cancer metastasis (Zhao et al. 2008; Kang et al. 2010). Thus, our findings are consistent with these reports and further suggest that the expression of Rho GDI is also correlated with prostate cancer metastasis. Consequently, Rho GDI should be considered as a diagnostic marker or new therapeutic target for cancer metastasis.

3. Experimental

3.1. Cell lines

SW480 is a human colorectal cancer cell line derived from a primary focus and SW620 is derived from a metastatic focus of the same patient. These cells were purchased from American Type Culture Collection and maintained at 37 °C using Leibovitz's L-15 medium (Wako) supplemented with 10% FCS. SW620-OK1 and -OK2 were established by the following procedure: 1×10^6 SW620 cells were injected into the spleens of nu/nu mice. After 8 weeks, SW620-OK1 was established from a liver metastatic focus. Furthermore, SW620-OK2 was established from SW620-OK1 using the same procedures.

3.2. 2D-DIGE analysis

Cell lysates were prepared from SW480 and SW620 and then solubilized with 7 M urea, 2 M thiourea, 4% CHAPS and 10 mM Tris-HCl (pH 8.5). The lysates were labeled at the ratio of 50 μg proteins: 400 pmol Cy3 or Cy5 protein-labeling dye (GE Healthcare Biosciences) in dimethylformamide according to the manufacturer's protocol. Briefly, the labelled samples were mixed with rehydration buffer (7 M urea, 2 M thiourea, 4% CHAPS, 2% DTT, 2% Pharmalyte (GE Healthcare Biosciences)) and applied to a 24-cm immobilized pH gradient gel strip (IPG-strip pH 4–7 NL) for separation in the first dimension. Samples for the spot-picking gel were prepared without labelling by Cy-dyes. For the second dimension separation, the IPG-strips were applied to SDS-PAGE gels (10% polyacrylamide and 2.7% N,N'-diallyltartardiamide gels). After electrophoresis, the gels were scanned with a laser fluoroimager (Typhoon Trio, GE Healthcare Biosciences). The spot-picking gel was scanned after staining with Deep Purple Total Protein Stain (GE Healthcare Biosciences). Quantitative analysis of protein spots was carried out with Decyder-DIA software (GE Healthcare Biosciences). For the antigen spots of interest, spots of 1 mm × 1 mm in size were picked using Ettan Spot Picker (GE Healthcare Biosciences).

3.3. In-gel tryptic digestion

Picked gel pieces were digested with trypsin as described below. The gel pieces were destained with 50% acetonitrile/50 mM NH_4HCO_3 for 20 min twice, dehydrated with 75% acetonitrile for 20 min, and then dried using a centrifugal concentrator. Next, 5 μl of 20 μl/ml trypsin (Promega) solution was added to each gel piece and incubated for 16 h at 37 °C. Three solutions were used to extract the resulting peptide mixtures from the gel pieces. First, 50 μl of 50% (v/v) acetonitrile in 0.1% (v/v) formic acid (FA) was added to the gel pieces, which were then sonicated for 5 min. Next, we collected the solution and added 80% (v/v) acetonitrile in 0.1% FA. Finally, 100% acetonitrile was added for the last extraction. The peptides were dried and then re-suspended in 10 μl of 0.1% FA.

3.4. Mass spectrometry and database search

Extracted peptides were analyzed by liquid chromatography Ultra High Resolution time-of-flight mass spectrometry (LC-UHR TOF/MS; maXis, Bruker Daltonics). The Mascot search engine (http://www.matrixscience.com) was initially used to query the entire theoretical tryptic peptide database as well as SwissProt (http://www.expasy.org/, a public domain database pro-

Table 2: Expression profile of Rho GDI in primary cancers with or without lymph node metastasis

	Number of Rho GDI positive cases (positive ratio)	
	in metastasis negative cases	in metastasis positive cases
Colon cancer*	11/14 (79%)	19/19 (100%)
Prostate cancer*	18/23 (78%)	11/11 (100%)

* $p < 0.05$: Mann Whitney U test

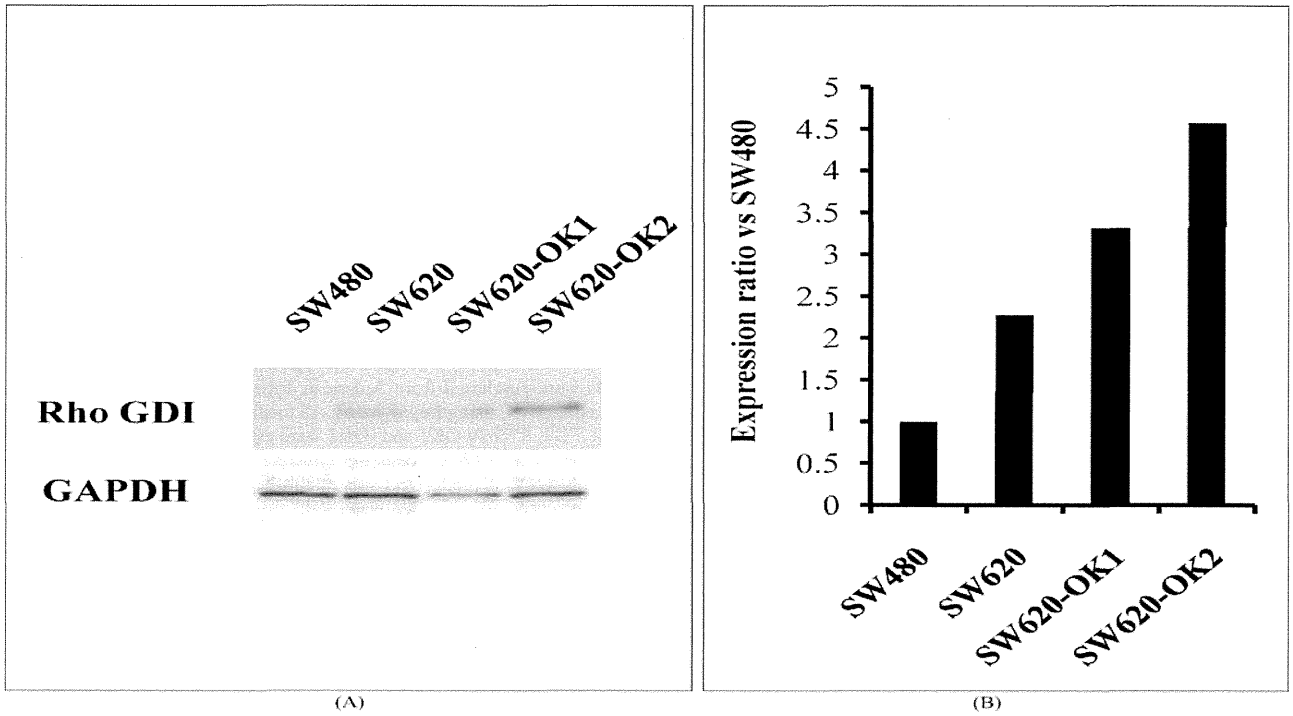

Fig. 2: Rho GDI expression levels in colon cancer cell lines with different metastatic abilities. Rho GDI expression levels in colon cancer cell lines (SW480, SW620, SW620-OK1, SW620-OK2) analyzed by western blotting (A). SW620-OK1, SW620-OK2 have been established as high metastatic sub-lines of SW620 using a mouse metastasis model. Intensity of the western blotting images was quantified by densitometry (B)

vided by the Swiss Institute of Bioinformatics). The search query assumed the following: (i) the peptides were monoisotopic (ii) methionine residues may be oxidized (iii) all cysteines are modified with iodoacetamide.

3.5. TMA Immunochemical staining

TMA slides with human colon cancer samples or multiple cancer samples (Biomax) were de-paraffinated in xylene and rehydrated in a graded series of ethanol washes. Heat-induced epitope retrieval was performed while maintaining the Target Retrieval Solution pH 9 (Dako) at the desired temperature according to manufacturer's instructions. After the treatment, endogenous peroxidase was blocked with 0.3% H_2O_2 in Tris-buffer saline (TBS) for 5 min. After washing twice with TBS, TMA slides were incubated with 10% BSA blocking solution for 30 min. The slides were then incubated with the anti-Rho GDI (Santa Cruz Biotechnology) for 60 min. After washing three times with wash buffer (Dako), each series of sections was incubated for 30 min with Envision + Dual Link (Dako). The reaction products were rinsed twice with wash buffer and then developed in liquid 3, 3'-diaminobenzidine (Dako) for 3 min. After the development, sections were counterstained with Mayer's hematoxylin. All procedures were performed using AutoStainer (Dako).

3.6. TMA Immunohistochemistry scoring

The optimized staining conditions for TMAs corresponding to human colon as well as multiple cancers were determined based on the co-existence of both positive and negative cells in the same tissue sample. Signals were considered positive when reaction products were localized in the expected cellular component. The criteria for scoring of stained tissues were as follows: the distribution score was 0 (0%), 1 (1–50%) or 2 (51–100%), indicating the percentage of positive cells among all tumor cells present in one tissue. The intensity of the signal (intensity score) was scored as 0 (no signal), 1 (weak), 2 (moderate) or 3 (marked). The distribution and intensity scores were then summed into a total score (TS) of TS0 (sum = 0), TS1 (sum = 2), TS2 (sum = 3), and TS3 (sum = 4–5). Throughout this study, TS0 or TS1 was regarded as negative, whereas TS2 or TS3 were regarded as positive.

3.7. Western Blot

Expression of Rho GDI in colon cancer cells was detected by anti-Rho GDI (Santa Cruz Biotechnology) and HRP conjugated anti-mouse IgG antibody (Sigma) using the ECL-plus system. Equal amounts of protein loading were confirmed by parallel β-actin immunoblotting, and signal quantification was performed by densitometric scanning.

Acknowledgements: This study was supported in part by Grants-in-Aid for Scientific Research from the Ministry of Education, Culture, Sports, Science and Technology of Japan, and from the Japan Society for the Promotion of Science (JSPS). This study was also supported in part by Health Labor Sciences Research Grants from the Ministry of Health, Labor and Welfare of Japan.

References

Bishop AL, Hall A (2000) Rho GTPases and their effector proteins. Biochem J 348: 241–255.

Davies RJ, Miller R, Coleman N (2005) Colorectal cancer screening: prospects for molecular stool analysis. Nat Rev Cancer 5: 199–209.

Etienne-Manneville S, Hall A (2002) Rho GTPases in cell biology. Nature 420: 629–635.

Hall A (1997). Rho GTPases and the Actin cytoskeleton. Science 279: 509–514.

Hanash S (2003) Disease proteomics. Nature 422: 226–232.

Imai S, Nagano K, Yoshida Y, Okamura T, Yamashita T, Abe Y, Yoshikawa T, Yoshioka Y, Kamada H, Mukai Y, Nakagawa S, Tsutsumi Y, Tsunoda S (2011). Development of an antibody proteomics system using a phage antibody library for efficient screening of biomarker proteins. Biomaterials 32: 162–169.

Kang S, Kim MJ, An H, Kim BG, Choi YP, Kang KS, Gao MQ, Park H, Na HJ, Kim HK, Yun HR, Kim DS, Cho NH (2010) Proteomic molecular portrait of interface zone in breast cancer. J Proteome Res 9: 5638–5645.

Liu R, Wang K, Yuan K, Wei Y, Huang C (2010) Integrative oncoproteomics strategies for anticancer drug discovery. Expert Rev Proteomics 7: 411–429.

Sahai E (2007). Illuminating the metastatic process. Nat Rev Cancer 7: 737–749.

Suehara Y, Tochigi N, Kubota D, Kikuta K, Nakayama R, Seki K, Yoshida A, Ichikawa H, Hasegawa T, Kaneko K, Chuman H, Beppu Y, Kawai A, Kondo T (2011) Secernin-1 as a novel prognostic biomarker candidate of synovial sarcoma revealed by proteomics. J Proteomics 74: 829–842.

Van Aelst L, D'Souza-Schorey C (1997) Rho GTPases and signaling networks. Genes Dev 11: 2295–2322.

Yoshida Y, Yamashita T, Nagano K, Imai S, Nabeshi H, Yoshikawa T, Yoshioka Y, Abe Y, Kamada H, Tsutsumi Y, Tsunoda S (2011) Limited expression of reticulocalbin-1 in lymphatic endothelial cells in lung tumor but not in normal lung. Biochem Biophys Res Commun 405: 610–614.

Zhao L, Wang H, Li J, Liu Y, Ding Y (2008) Overexpression of Rho GDP-dissociation inhibitor alpha is associated with tumor progression and poor prognosis of colorectal cancer. J Proteome Res 7: 3994–4003.

Biochemical and Biophysical Research Communications 421 (2012) 140–144

Contents lists available at SciVerse ScienceDirect

Biochemical and Biophysical Research Communications

journal homepage: www.elsevier.com/locate/ybbrc

Annexin A4 is a possible biomarker for cisplatin susceptibility of malignant mesothelioma cells

Takuya Yamashita [a,b,1], Kazuya Nagano [a,1], So-ichiro Kanasaki [a,b], Yuka Maeda [a,b], Takeshi Furuya [a,b], Masaki Inoue [a], Hiromi Nabeshi [b], Tomoaki Yoshikawa [a,b], Yasuo Yoshioka [a,b,c], Norio Itoh [b], Yasuhiro Abe [a], Haruhiko Kamada [a,c], Yasuo Tsutsumi [a,b,c], Shin-ichi Tsunoda [a,c,d,*]

[a] Laboratory of Biopharmaceutical Research, National Institute of Biomedical Innovation, 7-6-8 Saito-Asagi, Ibaraki, Osaka 567-0085, Japan
[b] Laboratory of Toxicology and Safety Science, Graduate School of Pharmaceutical Sciences, Osaka University, 1-6 Yamadaoka, Suita, Osaka 565-0871, Japan
[c] The Center for Advanced Medical Engineering and Informatics, Osaka University, 1-6 Yamadaoka, Suita, Osaka 565-0871, Japan
[d] Laboratory of Biomedical Innovation, Graduate School of Pharmaceutical Sciences, Osaka University, 1-6 Yamadaoka, Suita, Osaka 565-0871, Japan

ARTICLE INFO

Article history:
Received 27 March 2012
Available online 4 April 2012

Keywords:
Malignant mesothelioma
Cisplatin susceptibility
Annexin A4
Biomarker
Proteomics

ABSTRACT

Mesothelioma is a highly malignant tumor with a poor prognosis and limited treatment options. Although cisplatin (CDDP) is an effective anticancer drug, its response rate is only 20%. Therefore, discovery of biomarkers is desirable to distinguish the CDDP-susceptible versus resistant cases. To this end, differential proteome analysis was performed to distinguish between mesothelioma cells of different CDDP susceptibilities, and this revealed that expression of annexin A4 (ANXA4) protein was higher in CDDP-resistant cells than in CDDP-susceptible cells. Furthermore, ANXA4 expression levels were higher in human clinical malignant mesothelioma tissues than in benign mesothelioma and normal mesothelial tissues. Finally, increased susceptibility was observed following gene knockdown of ANXA4 in mesothelioma cells, whereas the opposite effect was observed following transfection of an ANXA4 plasmid. These results suggest that ANXA4 has a regulatory function related to the cisplatin susceptibility of mesothelioma cells and that it could be a biomarker for CDDP susceptibility in pathological diagnoses.

1. Introduction

Malignant mesothelioma is an aggressive neoplasm located on serosal membrane surfaces such as the pleura, and less frequently the peritoneum, and it has a poor outcome. The five-year survival rate is only about 5%. On the other hand, it is well known that asbestos is the major causative agent in the development of this disease [1–3]. Moreover, malignant mesothelioma takes 40–50 years to develop following exposure to asbestos. Because of its adiabatic potential, asbestos was commonly used as a building material in the 1960–1970s. Thus, an increase in mesothelioma patients is expected in the future. Patients with pleural malignant mesothelioma commonly present with an effusion associated with breathlessness that is often accompanied by chest-wall pain and a cough. After confirming the diagnosis, many patients are treated by intensive multidirectional approaches that combine cytoreductive surgery with intrapleural or intraperitoneal chemotherapy [4–8]. However, cytoreductive surgery is not always possible for patients with extensive intraperitoneal disease. Thus, the role of chemotherapy in malignant mesothelioma is critically important.

CDDP is an extensively used anticancer drug for the treatment of malignant mesothelioma, although the response rate is only about 20% [9–12]. A major problem with CDDP treatment of malignant mesothelioma patients is the development of CDDP insusceptibility. Thus, there is an urgent need to further our understanding of the pathogenesis of malignant mesothelioma, particularly with respect to the expression of proteins that confer drug susceptibility, in order to develop novel therapeutic strategies. In this study, a proteomic analysis was performed using high- and low-CDDP-susceptible malignant mesothelioma cells to identify candidate proteins associated with CDDP susceptibility.

2. Materials and methods

2.1. Cells

H28, H2052, H2452, H226 and MSTO-221H were purchased from American Type Culture Collection and maintained in RPMI1640 medium (Wako) containing 10% fetal calf serum (Biowest). Human mesothelial cells (HMC) were purchased from

* Corresponding author at: Laboratory of Biopharmaceutical Research, National Institute of Biomedical Innovation, 7-6-8 Saito-Asagi, Ibaraki, Osaka 567-0085, Japan. Fax: +81 72 641 9817.
E-mail address: tsunoda@nibio.go.jp (S.-i. Tsunoda).
[1] These authors contributed equally to this work.

0006-291X/$ - see front matter © 2012 Elsevier Inc. All rights reserved.
http://dx.doi.org/10.1016/j.bbrc.2012.03.144

Sciencell and cultured in Mesothelial Cell Growth Medium (ZenBio) under a 5% CO_2 atmosphere at 37 °C.

2.2. Measurement of cisplatin susceptibility in malignant mesothelioma cells

Malignant mesothelioma cells were seeded into 96-well microplates and cultured overnight. Various concentrations of CDDP were added to each well, the plates were incubated for 24 h, and cell viability was measured using Cell count reagent SF (Nacalai tesque). Absorbance was measured using a microplate reader (Bio-Rad) at test and reference wavelengths of 450 and 650 nm, respectively.

2.3. Proteomic analysis using two dimensional differential in-gel electrophoresis

For proteomic analysis, quantitative analysis was performed using two dimensional differential in-gel electrophoresis (2D-DIGE). Cell lysates were prepared from H28 and H2052 and then solubilized with 7 M urea, 2 M thiourea, 4% CHAPS and 10 mM Tris–HCl (pH 8.5). The lysates were labeled at the ratio of 50 μg proteins: 400 pmol Cy3 or Cy5 protein-labeling dye (GE Healthcare Biosciences) in dimethylformamide according to the manufacturer's protocol. The labelled samples were mixed with rehydration buffer (7 M urea, 2 M thiourea, 4% CHAPS, 2% DTT, 2% Pharmalyte (GE Healthcare Biosciences)) and applied to a 24-cm immobilized pH gradient gel strip (IPG-strip pH 4–7) for separation in the first dimension. For the second dimension separation, the IPG-strips were treated with iodoacetamide and applied to SDS–PAGE gels (10% polyacrylamide and 2.7% *N,N′*-diallyltartardiamide gels). After electrophoresis, the gels were scanned with a laser fluoroimager (Typhoon Trio, GE Healthcare Biosciences). The spot-picking gel was scanned after staining with Deep purple total protein stain (GE Healthcare Biosciences). Quantitative analysis of protein spots was carried out with Decyder-DIA software (GE Healthcare Biosciences). For the antigen spots of interest, spots of 1 mm × 1 mm in size were picked using Ettan Spot Picker (GE Healthcare Biosciences).

2.4. In-gel tryptic digestion

Picked gel pieces were destained with 50% acetonitrile/50 mM NH_4HCO_3 for 20 min twice, dehydrated with 75% acetonitrile for 20 min, and then dried using a centrifugal concentrator. Five microliter of 20 μg/ml trypsin (Promega) solution was added to each gel piece and the pieces were incubated for 16 h at 37 °C. The digested peptides were extracted sequentially using 50%, 80%, and 100% acetonitrile and then dried before being suspended in 10 μl of 0.1% formic acid.

2.5. Mass spectrometry and database search

Extracted peptides were analyzed by liquid chromatography ultra high resolution time-of-flight mass spectrometry (LC-UHR TOF-MS/MS; maXis, Bruker Daltonics). The Mascot search engine (http://www.matrixscience.com) was initially used to query the entire theoretical tryptic peptide database as well as SwissProt (http://www.expasy.org/, a public domain database provided by the Swiss Institute of Bioinformatics). The search query assumed the following: (i) the peptides were mono-, di- or tri-isotopic, (ii) methionine residues may be oxidized, (iii) all cysteines were modified with carbamidomethyl.

2.6. Western blot

The cell lysates were separated in 10% SDS–polyacrylamide gels and transferred to Immobilon membranes (Millipore). After blocking by 4% block ace (DS Pharma Biomedical) for 1 h at room temperature, the blots were reacted with primary antibodies in a buffer containing 0.4% block ace, and then with the appropriate peroxidase-conjugated secondary antibodies in the same buffer. Expression of ANXA4 in malignant mesothelioma cells was detected by mouse anti-human ANXA4 (Abnova: 1D3) followed by an HRP-conjugated anti-mouse IgG antibody (Sigma–Aldrich) using the ECL-plus system (GE Healthcare Biosciences). Equal amounts of protein loading were confirmed by parallel β-actin immunoblotting, and signal quantification was performed by densitometric scanning.

2.7. Immunohistochemistry staining

Human mesothelioma and normal tissue sections were deparaffinated in xylene and rehydrated in a graded series of ethanol dilutions. Heat-induced epitope retrieval was performed by incubating at different temperatures following the manufacturer's instructions using Target Retrieval Solution pH 9 (Dako). After heat-induced epitope retrieval treatment, endogenous peroxidase was blocked with a peroxidase blocking reagent (Dako). Following peroxidase blocking, the slides were incubated with 10% bovine serum albumin (BSA) solution for 30 min at room temperature. The slides were then incubated for 60 min with anti-human ANXA4 monoclonal antibody (9 μg/ml) in 3% BSA at room temperature. After washing 3 times with wash buffer (Dako), the slides were incubated for 30 min with ENVISION + Dual Link (Dako) at room temperature. They were then washed final 3 times and stained with 3,3′-diaminobenzidine. After development, the slides were lightly counterstained with Mayer's hematoxylin and mounted with resinous mounting medium.

2.8. Cisplatin susceptibility in cells transfected with ANXA4-siRNA and ANXA4-plasmid

H28 was transfected with ANXA4-siRNA (target sequence: AAGGATATCACAGAAGGATAT, Qiagen) using Hyperfect reagent (Qiagen) according to the manufacturer's instructions. In contrast, H2052 was transfected with ANXA4-pcDNA 3.1 (a gift from Naka T: Laboratory for Immune Signal, National Institute of Biomedical Innovation) using FuGENE HD transfection reagent (Roche). After transfection, the cells were treated with various concentrations of CDDP for 36 h (ANXA4-siRNA) or 24 h (ANXA4-pcDNA 3.1). Cell viability was measured as described above.

2.9. Statistical analysis

Differences in tumor volumes between the control and target groups were compared using the unpaired Student's *t*-test.

3. Results

3.1. CDDP susceptibility in malignant mesothelioma cells

Cell viability following CDDP treatment was examined to determine which cell lines had higher or lower susceptibility to CDDP. Among five tested mesothelioma cell lines, H2052 was the most and H28 the least susceptible cell line (Fig. 1). The IC_{50} values of H28, H2052, H2452, H226 and MSTO-221H were 154.5, 27.8, 66.0, 87.5 and 49.5 μM, respectively.

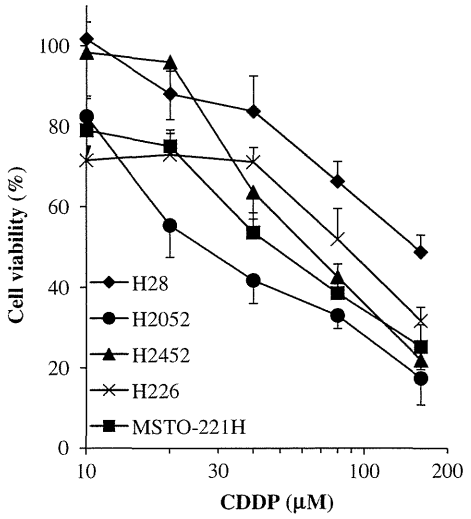

Fig. 1. Susceptibility of malignant mesothelioma cells to CDDP. Mesothelioma cells, H28, H2052, H2452, H226 and MSTO-221H were cultured with various concentrations of CDDP for 24 h 37 °C under 5% CO_2. Cell viability was assayed using the WST-8 assay. Maximal cell viability (100%) was obtained by incubating cells without CDDP. Data are shown as means and standard deviations ($n = 4$).

3.2. Identification of differentially expressed proteins by 2D-DIGE and MS

In order to search for CDDP susceptibility-related proteins, differential proteome analysis between H2052 and H28 cell lines was performed to search for CDDP susceptibility-related proteins (Fig. 2). Quantitative image analysis indicated that a total of eight protein spots representing > 2.0-fold alteration in expression were found and then identified by MS analysis (Table 1). Among those eight proteins, we focused on ANXA4 because this protein plays an important role in membrane stability. Previous reports have indicated that ANXA4 is associated with chemoresistance against platinum-based anticancer drugs in human lung, colon [13] and ovarian cancer [14].

3.3. ANXA4 expression analysis in human malignant mesothelioma cells and mesothelial tissues

Correlations between the expression levels in five malignant mesothelioma cell lines with CDDP-susceptibility were examined using western blot analysis to validate the identified proteins as CDDP susceptibility-related proteins. ANXA4 was expressed at a higher level in H28 cells relative to the other four CDDP-susceptible malignant mesothelioma cell lines (Fig. 3A and B). Expression of ANXA4 in human mesothelial tissue was analyzed by immunohistochemistry staining with an anti-human ANXA4 monoclonal antibody. Fig. 3C indicates that ANXA4 was expressed at higher levels in human malignant mesothelioma tissues than in benign mesothelioma tissues and normal mesothelial tissues.

3.4. Gene regulation of ANXA4 in malignant mesothelioma cells by knockdown and overexpression

ANXA4-siRNA and ANXA4-pcDNA 3.1 were next transfected to H28 and H2052 before CDDP treatment to evaluate correlations between ANXA4 expression levels and CDDP susceptibility. The IC_{50} values of [H28/non treat: H28/control-siRNA: H28/ANXA4-siRNA] were [80.0 μM: 71.8 μM: 15.5 μM] and [H2052/control-pcDNA 3.1: [H2052/ANXA4-pcDNA 3.1] were [55.2 μM: 89.7 μM], respectively (Fig. 4A–D). These results suggested that the CDDP susceptibility of H28 cells was increased by ANXA4-siRNA transfection and that of H2052 cells was decreased by ANXA4-pcDNA 3.1 transfection.

4. Discussion

In this study, a proteomic analysis was performed based on 2D-DIGE using malignant mesothelioma cell lines to identify candidate proteins associated with CDDP susceptibility (Figs. 1 and 2). Eight proteins that were differentially expressed in H28 cells compared with H2052 cells were identified (Table 1). ANXA4 was found to be expressed at a higher level in H28 cells relative to levels in CDDP-susceptible malignant mesothelioma cells by western blot

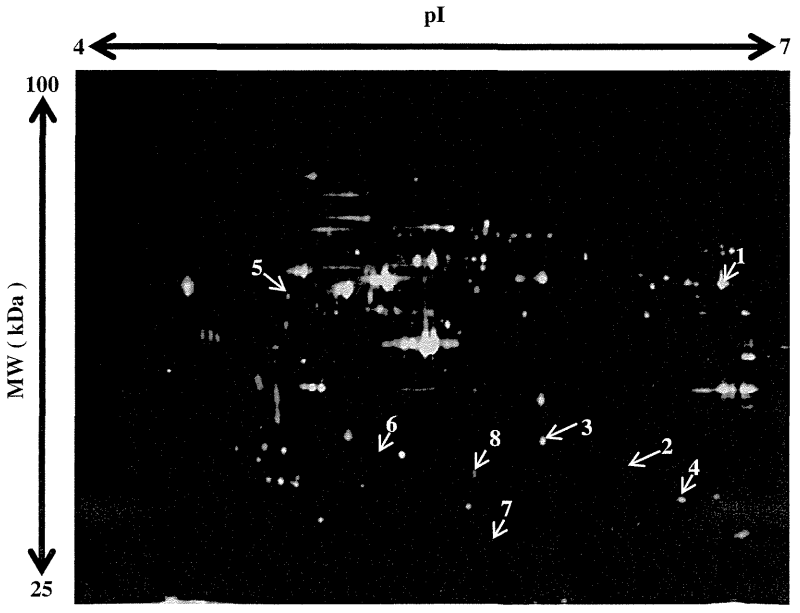

Fig. 2. 2D-DIGE image of fluorescently labeled proteins from human mesothelioma cell lines H28 and H2052. Proteins from high- and low-susceptible mesothelioma cells (H2052, H28) were labeled with cy3 and cy5, respectively, and 2D electrophoresis was performed. The differentially expressed spots in H28 indicated by white arrows were then identified by LC-TOF-MS/MS. Table 1 contains additional information about the identified proteins.

Table 1
Proteins expressed at higher or lower levels in H28 compared to H2052.

No.	Accession number	Protein name	pI	MW (kDa)	Expression ratio (H28/H2052)
1	P11413	Glucose-6-phosphate 1-dehydrogenase	6.4	59.3	21.0
2	P78417	Glutathione *S*-transferase omega-1	6.2	27.6	7.4
3	P09525	Annexin A4	5.6	35.9	3.6
4	P30041	Peroxiredoxin-6	6.0	25.0	3.5
5	Q09028	Histone-binding protein RBBP4	4.7	47.7	3.0
6	P07195	L-lactate dehydrogenase B chain	5.7	36.6	2.9
7	P32119	Peroxiredoxin-2	5.7	21.9	0.03
8	Q9Y696	Chloride intracellular channel protein 4	5.5	28.8	0.13

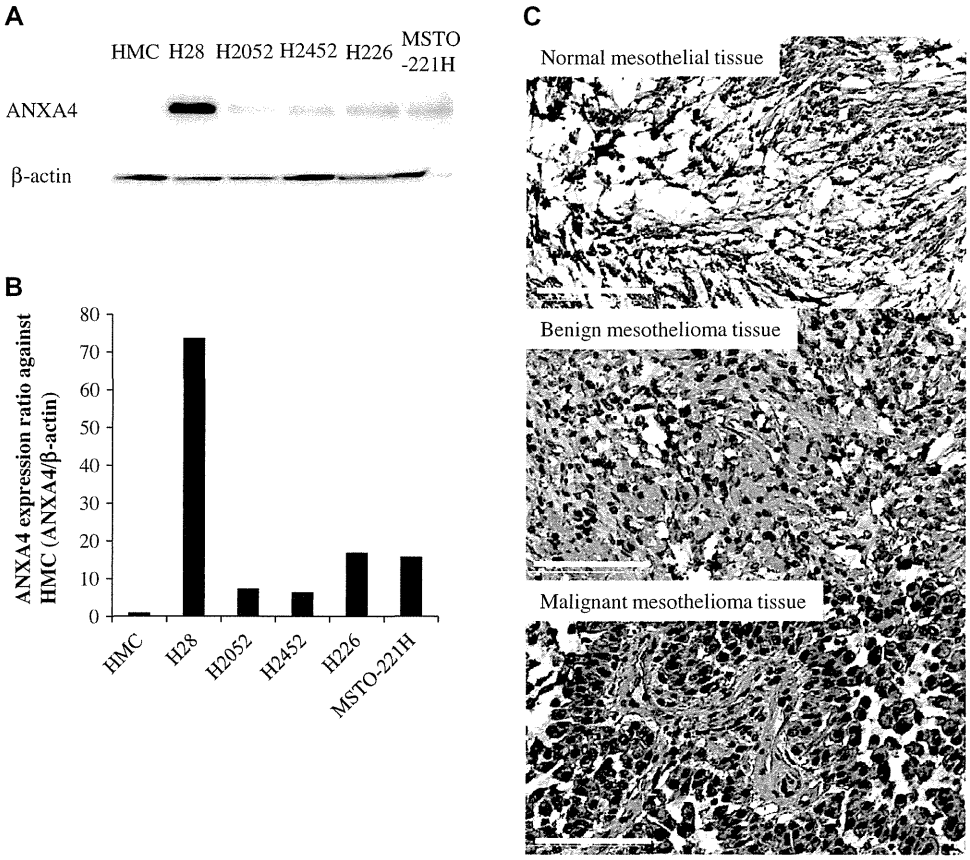

Fig. 3. ANXA4 expression analysis in human malignant mesothelioma cells and mesothelial tissues. ANXA4 expression levels in human primary mesothelial cells, HMC, and mesothelioma cell lines (H28, H2052, H2452, H226, MSTO-221H) were analyzed by western blotting (A). Intensity of the western blotting images was quantified by densitometry (B). Expression of ANXA4 in human mesothelial tissues was analyzed by immunostaining using an anti-human ANXA4 antibody (C). Top, middle and bottom panels are normal mesothelial, benign and malignant mesothelioma tissues, respectively. The tissue sections were counterstained using hematoxylin. Representative 400 × photomicrographs presented (bar: 100 μm).

analysis (Fig. 3A and B). Furthermore, ANXA4 was expressed in malignant mesothelioma tissue but not in benign mesothelial tumor and normal mesothelial tissues (Fig. 3C). Thus, ANXA4 was expressed in CDDP-susceptible malignant mesothelioma cells and specifically in malignant mesothelioma tissues. These results indicate that ANXA4 expression in malignant mesothelioma cells may be correlated with CDDP susceptibility, although this relationship must be validated in future studies of human clinical malignant mesothelial cases. The CDDP susceptibility of H28 cells was actually increased by ANXA4 knockdown, and that of H2052 cells was decreased by ANXA4 overexpression (Fig. 4). Thus, these results suggest that ANXA4 plays an important role in chemoresistance against CDDP.

ANXA4 has already been characterized as a regulator of cell membranes with calcium dependency [15–17]. Recently, some studies have reported the protein is associated with membrane permeability [18], ion channels [19] and exocytosis [20,21]. These observations may explain in part the correlation of ANXA4 with modulation of drug susceptibility in cancer cells.

This study demonstrates for the first time elevated ANXA4 protein expression in malignant mesothelioma cells that have less susceptibility to CDDP. *In vitro* evaluation of drug susceptibility against CDDP in malignant mesothelioma cells derived from cancer patients would be important in clinical conditions because doctors as well as patients wish to avoid treatment with inefficacious drugs. Consequently, the susceptibility of a given patient against CDDP could be confirmed by analyzing the expression level of ANXA4 in malignant mesothelioma patients at the time of diagnosis. Furthermore, if ANXA4 expression could be blocked specifically in malignant mesothelioma cells by nucleic acid drugs such as siRNA, this procedure would prove useful in clinical situations involving CDDP treatment. The present study may contribute to

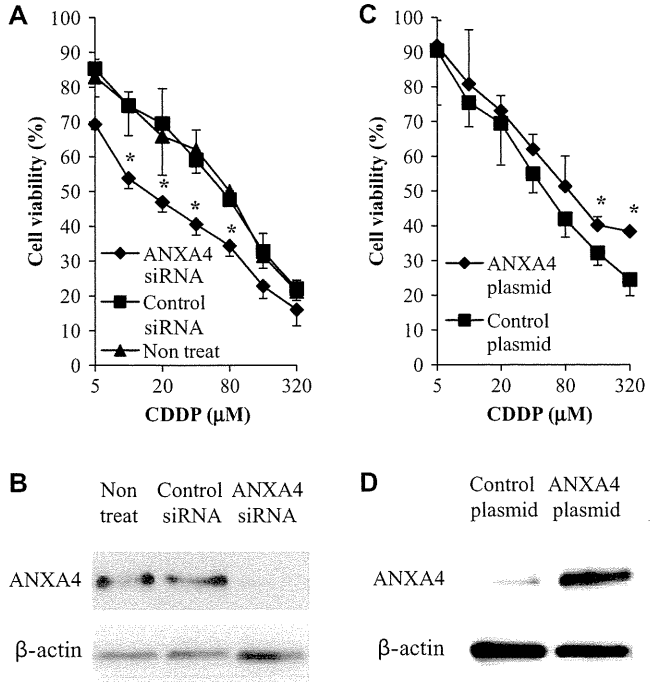

Fig. 4. The effect of ANXA4 gene knockdown and overexpression on CDDP susceptibility in malignant mesothelioma cells. Transfection of ANXA4 siRNA or plasmid into malignant mesothelioma cells confers resistance to CDDP. Cell survival after 24 h treatment of H28/ANXA4 siRNA or H2052/ANXA4 plasmid with different concentrations of CDDP (A and C). Expression of ANXA4 was analyzed by western blot analysis (B and D). Data are shown as means and standard deviations ($n = 4$). *$P < 0.05$ (Control siRNA or plasmid vs. ANXA4 siRNA or plasmid).

establishment of a new therapeutic strategy for malignant mesothelioma patients by suggesting a novel diagnostic and therapeutic target.

Acknowledgments

This study was supported in part by Grants-in-Aid for Scientific Research from the Ministry of Education, Culture, Sports, Science and Technology of Japan, and from the Japan Society for the Promotion of Science (JSPS). This study was also supported in part by Health Labor Sciences Research Grants from the Ministry of Health, Labor and Welfare of Japan and by Health Sciences Research Grants for Research on Publicly Essential Drugs and Medical Devices from the Japan Health Sciences Foundation.

References

[1] W.N. Rom, W.D. Travis, A.R. Brody, Cellular and molecular basis of the asbestos-related diseases, Am. Rev. Respir. Dis. 143 (1991) 408–422.
[2] N.H. Heintz, Y.M. Janssen-Heininger, B.T. Mossman, Asbestos, lung cancers, and mesotheliomas: from molecular approaches to targeting tumor survival pathways, Am. J. Respir. Cell Mol. Biol. 42 (2010) 133–139.
[3] Consensus Report: Asbestos, asbestosis, and cancer: the Helsinki criteria for diagnosis and attribution. Scand. J. Work Environ. Health 23 (1997) 311–316.
[4] T.D. Yan, L. Welch, D. Black, P.H. Sugarbaker, A systematic review on the efficacy of cytoreductive surgery combined with perioperative intraperitoneal chemotherapy for diffuse malignancy peritoneal mesothelioma, Ann. Oncol. 18 (2007) 827–834.
[5] E. Chailleux, D. Pioche, S. Chopra, G. Dabouis, P. Germaud, A.Y. De Lajartre, M. De Lajartre, Prognostic factors in diffuse malignant pleural mesothelioma: a study of 167 patients, Chest 93 (1988) 159–162.
[6] K.S. Sridhar, R. Doria, W.A. Raub Jr., R.J. Thurer, M. Saldana, New strategies are needed in diffuse malignant mesothelioma, Cancer 70 (1992) 2969–2979.
[7] M. Markman, D. Kelsen, Efficacy of cisplatin-based intraperitoneal chemotherapy as treatment of malignant peritoneal mesothelioma, J. Cancer Res. Clin. Oncol. 118 (1992) 547–550.
[8] G.H. Eltabbakh, M.S. Piver, R.E. Hempling, F.O. Recio, M.E. Intengen, Clinical picture, response to therapy, and survival of women with diffuse malignant peritoneal mesothelioma, J. Surg. Oncol. 70 (1999) 6–12.
[9] T. Berghmans, M. Paesmans, Y. Lalami, I. Louviaux, S. Luce, C. Mascaux, A.P. Meert, J.P. Sculier, Activity of chemotherapy and immunotherapy on malignant mesothelioma: a systematic review of the literature with meta-analysis, Lung. Cancer 38 (2002) 111–121.
[10] H.J. Lerner, D.A. Schoenfeld, A. Martin, G. Falkson, E. Borden, Malignant mesothelioma: The Eastern Cooperative Oncology Group (ECOG) experience, Cancer 52 (1983) 1981–1985.
[11] D.M. Mintzer, D. Kelsen, D. Frimmer, R. Heelan, R. Gralla, Phase II trial of high-dose cisplatin in patients with malignant mesothelioma, Cancer Treat Rep. 69 (1985) 711–712.
[12] B.L. Zidar, S. Green, H.I. Pierce, R.W. Roach, S.P. Balcerzak, L. Militello, A phase II evaluation of cisplatin in unresectable diffuse malignant mesothelioma: a Southwest Oncology Group Study, Invest New Drugs 6 (1988) 223–226.
[13] E.K. Han, S.K. Tahir, S.P. Cherian, N. Collins, S.C. Ng, Modulation of paclitaxel resistance by annexin IV in human cancer cell lines, Br. J. Cancer 83 (2000) 83–88.
[14] A. Kim, T. Enomoto, S. Serada, Y. Ueda, T. Takahashi, B. Ripley, T. Miyatake, M. Fujita, C.M. Lee, K. Morimoto, M. Fujimoto, T. Kimura, T. Naka, Enhanced expression of Annexin A4 in clear cell carcinoma of the ovary and its association with chemoresistance to carboplatin, Int. J. Cancer 125 (2009) 2316–2322.
[15] M.A. Kaetzel, P. Hazarika, J.R. Dedman, Differential tissue expression of three 35-kDa annexin calcium-dependent phospholipid-binding proteins, J. Biol. Chem. 264 (1989) 14463–14470.
[16] G. Zanotti, G. Malpeli, F. Gliubich, C. Folli, M. Stoppini, L. Olivi, A. Savoia, R. Berni, Structure of the trigonal crystal form of bovine annexin IV, Biochem. J. 329 (1998) 101–106.
[17] M.A. Kaetzel, Y.D. Mo, T.R. Mealy, B. Campos, W. Bergsma-Schutter, A. Brisson, J.R. Dedman, B.A. Seaton, Phosphorylation mutants elucidate the mechanism of annexin IV-mediated membrane aggregation, Biochemistry 40 (2001) 4192–4199.
[18] W.G. Hill, M.A. Kaetzel, B.K. Kishore, J.R. Dedman, M.L. Zeidel, Annexin A4 reduces water and proton permeability of model membranes but does not alter aquaporin 2-mediated water transport in isolated endosomes, J. Gen. Physiol. 121 (2003) 413–425.
[19] M.A. Kaetzel, H.C. Chan, W.P. Dubinsky, J.R. Dedman, D.J. Nelson, A role for annexin IV in epithelial cell function. Inhibition of calcium-activated chloride conductance, J. Biol. Chem. 269 (1994) 5297–5302.
[20] H. Sohma, C.E. Creutz, S. Gasa, H. Ohkawa, T. Akino, Y. Kuroki, Differential lipid specificities of the repeated domains of annexin IV, Biochim. Biophys. Acta 1546 (2001) 205–215.
[21] A. Piljic, C. Schultz, Annexin A4 self-association modulates general membrane protein mobility in living cells, Mol. Biol. Cell 17 (2006) 3318–3328.

blood

2010 115: 736-744
Prepublished online November 10, 2009;
doi:10.1182/blood-2009-08-239004

In vivo biotinylation of the vasculature in B-cell lymphoma identifies BST-2 as a target for antibody-based therapy

Christoph Schliemann, Christoph Roesli, Haruhiko Kamada, Beatrice Borgia, Tim Fugmann, Wolfram Klapper and Dario Neri

Blood (print ISSN 0006-4971, online ISSN 1528-0020), is published weekly by the American Society of Hematology, 2021 L St, NW, Suite 900, Washington DC 20036.

In vivo biotinylation of the vasculature in B-cell lymphoma identifies BST-2 as a target for antibody-based therapy

*Christoph Schliemann,[1] *Christoph Roesli,[1] Haruhiko Kamada,[1,2] Beatrice Borgia,[1] Tim Fugmann,[1] Wolfram Klapper,[3] and Dario Neri[1]

[1]Institute of Pharmaceutical Sciences, Department of Chemistry and Applied Biosciences, ETH Zurich, Zurich, Switzerland; [2]Laboratory of Pharmaceutical Proteomics, National Institute of Biomedical Innovation, Osaka, Japan; and [3]Institute of Pathology, Section Hematopathology and Lymph Node Registry, University Hospital Schleswig-Holstein, Kiel, Germany

The discovery of accessible markers of lymphoma may facilitate the development of antibody-based therapeutic strategies. Here, we describe the results of a chemical proteomic study, based on the in vivo biotinylation of vascular proteins in lymphoma-bearing mice followed by mass spectrometric and bioinformatic analysis, to discover proteins expressed at the tissue-blood border of disseminated B-cell lymphoma. From a list of 58 proteins, which were more than 10-fold up-regulated in nodal and extranodal lymphoma lesions compared with their levels in the corresponding normal host organs, we validated BST-2 as a novel vascular marker of B-cell lymphoma, using immunochemical techniques and in vivo biodistribution studies. Furthermore, targeting BST-2 with 2 independent monoclonal antibodies delayed lymphoma growth in a syngeneic mouse model of the disease. The results of this study delineate a strategy for the treatment of systemic B-cell lymphoma in humans and suggest that anti–BST-2 antibodies may facilitate pharmacodelivery approaches that target the tumor-stroma interface. (Blood. 2010;115: 736-744)

Introduction

Monoclonal antibodies are increasingly being used in modern anticancer therapy either as intact immunoglobulins or as carriers for the selective delivery of bioactive molecules (eg, drugs with cleavable linkers, radionuclides, cytokines) to the tumor site, thereby minimizing exposure to noninvolved organs.[1-6] Initially, site-directed cancer therapies have mainly aimed at targeting antigens expressed on the surface of cancer cells. However, tumor cells embedded in large tumor masses are not readily accessible to antibodies from the bloodstream,[7] an obstacle that may reduce their in vivo therapeutic efficacy despite a sufficient activity in vitro. Recently, pharmacodelivery strategies have been developed that target molecules expressed in tumor blood vessels or in the tumor stroma.[1,3,6] Indeed, structures in the immediate vicinity of the tissue-blood border are not only inherently accessible to blood-borne agents but also allow some unique therapeutic options. For example, the angiogenic endothelium appears exceptionally suited for the selective shutdown of a tumor's blood supply.[8] Components of the subendothelial extracellular matrix are often more abundantly expressed, permitting an efficient antibody-mediated deposition of bioactive payloads at the tumor site.[9-14]

Antibody-based pharmacodelivery strategies are particularly attractive for the therapy of hematologic malignancies, in light of the fact that patients with leukemias or lymphomas commonly experience serious side effects from conventional induction chemotherapies. The advent of monoclonal antibodies specific to certain CD antigens represented a significant step toward a more specific therapy of these malignancies, either unconjugated (eg, rituximab or alemtuzumab) or as carriers for cytotoxic drugs (eg, gemtuzumab ozogamicin) or radionuclides (eg, ibritumomab tiuxetan).[15] Whereas cell-surface antigens have been extensively characterized and exploited for antibody-based targeted therapies over the years,[15,16] lymphoma-specific markers expressed in the vascular[13,14] or stromal[17] compartment have attracted less attention so far. Very recently, the extra domain B (EDB) of oncofetal fibronectin, a marker of angiogenesis, has been proposed as an antigen for vascular-targeted pharmacodelivery strategies in lymphoma, based on immunohistochemical findings and on preclinical and clinical studies with the EDB-targeted immunocytokine L19-IL2 and the radiolabeled antibody ^{131}I-L19.[13,14] Indeed, this radiopharmaceutical could eradicate aggressive lymphomas in patients who had previously failed to respond to multiple lines of chemotherapy and radiotherapy. L19-IL2 was found to potently synergize with the anti-CD20 antibody rituximab, eradicating localized and systemic B-cell lymphomas in mice that could not be cured with either agent alone.[13] These promising results provide a strong motivation to continue the search for vascular markers of lymphoma that may be drugged with antibodies.

Our group has developed a general chemical proteomics approach for the identification of proteins that are readily accessible from the bloodstream. The method relies on the covalent labeling of vascular proteins by in vivo perfusion of tumor-bearing animals[18,19] or by ex vivo perfusion of surgically resected human organs,[20] using reactive ester derivatives of biotin. The resulting biotinylated proteins can be efficiently recovered from normal and pathologic tissues by purification on

Submitted August 17, 2009; accepted October 15, 2009. Prepublished online as *Blood* First Edition paper, November 10, 2009; DOI 10.1182/blood-2009-08-239004.

*C.S. and C.R. contributed equally to this study and share first authorship.

The online version of this article contains a data supplement.

The publication costs of this article were defrayed in part by page charge payment. Therefore, and solely to indicate this fact, this article is hereby marked "advertisement" in accordance with 18 USC section 1734.

streptavidin resins.[19] On-resin proteolytic digestion of biotinylated proteins, nano–high-performance liquid chromatography (HPLC) separation of resulting peptides, and their identification and relative quantification in the presence of internal standards by tandem mass spectrometry,[21] allow the characterization of atlases of circulation-accessible proteins in normal organs and at sites of disease, thus facilitating the discovery of novel markers of pathology.

Here, we describe the in vivo biotinylation of immunocompetent mice bearing syngeneic disseminated A20 B-cell lymphoma, using a terminal perfusion procedure. The A20 lymphoma model is known to closely mimic histopathologic aspects and the anatomic distribution of large B-cell lymphoma in humans, recapitulating nodal and extranodal tumor growth in various organs.[22] Comparative proteomic analyses of lymphoma lesions and their corresponding host organs allowed the identification of a repertoire of differentially expressed bloodstream-accessible proteins. One highly promising candidate, BST-2, has been investigated in detail, revealing a restricted expression at lymphoma vascular sites, which could be targeted in vivo using anti–BST-2 antibodies. Furthermore, 2 anti–BST-2 monoclonal antibodies substantially reduced tumor growth in vivo, thus suggesting that this antigen may be suitable for therapeutic strategies both with intact immunoglobulins and with judiciously chosen antibody derivatives.

Methods

Animal model

The A20 murine B-cell lymphoma cell line was purchased from ATCC. Six- to 8-week-old female BALB/c mice were obtained from Charles River Laboratories. Systemic B-cell lymphoma was induced by injection of 2×10^6 A20 cells into the tail vein.[22] Twenty-four to 26 days after injection, 12 mice bearing disseminated A20 lymphoma and 6 age-matched healthy mice were subjected to the in vivo protein biotinylation procedure. All animal experiments were approved by the Swiss Federal Veterinary Office (license 198/2005).

In vivo protein biotinylation

In vivo biotinylation experiments were performed as previously described.[18,19] After perfusion with the reactive ester derivative of biotin, organs and tumors were excised and specimens were either snap-frozen for preparation of organ homogenates or embedded in cryoembedding compound (Thermo Fisher Scientific) and frozen for histochemical analysis.

Preparation of protein extracts

Lymphoma lesions and their corresponding host organs were resuspended in lysis buffer (2% sodium dodecyl sulfate [SDS], 50mM Tris, 10mM ethylenediaminetetraacetic acid, CompleteE proteinase inhibitor cocktail [Roche Diagnostics] in phosphate-buffered saline [PBS], pH 7.4), using 40 μL/mg tissue. The specimens were then homogenized using an Ultra-Turrax T8 disperser (IKA-Werke) and sonicated using a Vibra-cell (Sonics), followed by 15 minutes of incubation at 95°C and 20 minutes' centrifugation at 15 000*g*. The resulting supernatants ("total protein extracts") were used for the subsequent capture step on streptavidin-resin. The protein concentration of the total protein extracts was determined with the BCA Protein Assay Reagent Kit (Thermo Fisher Scientific).

Purification of biotinylated proteins

For each sample, 400 μL of streptavidin-sepharose (GE Healthcare) slurry were washed 3 times with buffer A (1% NP40, 0.1% SDS in PBS), pelleted, and mixed with 5 mg of total protein extract. The capture of biotinylated proteins was allowed to proceed for 2 hours at room temperature in a revolving mixer. The supernatant was removed, and the resin was washed 3 times with buffer A, twice with buffer B (0.1% SDS, 2M NaCl in PBS, 40°C), and 8 times with digestion buffer (50mM Tris-HCl, 1mM $CaCl_2$, pH 8.0). Finally, the resin was resuspended in 200 μL of digestion buffer and 20 μL of sequencing grade modified porcine trypsin (stock solution of 80 ng/μL in digestion buffer; Promega) were added. Tryptic digestion was carried out overnight at 37°C under constant agitation. Peptides were desalted, purified, and concentrated with C_{18} microcolumns (Varian Inc). After lyophilization, peptides were stored at −20°C.

Nanocapillary reverse-phase HPLC with online fraction spotting onto MALDI plates

Tryptic peptides were separated by reverse-phase HPLC using an UltiMate nanoscale LC system and a FAMOS microautosampler (LC Packings) controlled by the Chromeleon software (Dionex). Mobile phase A consisted of 5% acetonitrile and 0.1% trifluoroacetic acid (TFA) in water, mobile phase B of 80% acetonitrile, and 0.1% TFA in water. The flow rate was 300 nL/minute. Lyophilized peptides derived from the digestion of biotinylated protein affinity purified from 2 mg of total protein were dissolved in 5 μL of buffer A and loaded on the column (inner diameter, 75 μm; length, 15 cm; filled with C_{18} PepMap 100, 3-μm, 100-Å beads; LC Packings). The peptides were eluted with a gradient of 0% B for 3 minutes, 0% to 52% B for 82 minutes, 52% to 100% B for 10 minutes, and 100% B for 5 minutes; the column was equilibrated with 100% A for 20 minutes before analyzing the next sample. Eluting fractions were mixed with a solution of 3 mg/mL α-cyano-4-hydroxycinnamic acid, 277pmol/mL of each of the 4 internal standard peptides ([des-arg^9]-bradykinin, neurotensin, angiotensin I, and adrenocorticotropic hormone fragment 1-17; all from Sigma-Aldrich), 0.1% TFA, and 70% acetonitrile in water and deposited on a blank matrix-assisted laser desorption/ionization (MALDI) target plate (416 spots per sample) using an online Probot system (Dionex). The final concentration of each internal standard peptide was 50fmol per spot.

MALDI-TOF/TOF mass spectrometry

MALDI–time-of-flight (TOF)/TOF analysis was carried out with the 4800 MALDI TOF/TOF Analyzer (Applied Biosystems). All spectra were acquired with a solid-state laser (355 nm) at a laser repetition rate of 200 Hz. After measuring all samples in the mass spectrometry (MS) mode, a maximum of 15 precursors per spot were automatically selected for subsequent fragmentation by collision-induced dissociation. Resulting spectra were processed and analyzed using both the ProteinPilot software (Applied Biosystems; Paragon algorithm) and the Global Protein Server Workstation (Applied Biosystems; using internal MASCOT Matrix Science), for matching MS and MS/MS data against databases of in silico digested proteins. The data obtained were screened against a database of all mouse proteins downloaded from the European Bioinformatics Institute homepage (ftp.ebi.ac.uk/pub/databases/SPproteomes/fasta/proteomes/59.M_musculus.fasta.gz). The following settings were used for the identification of peptides and proteins: (1) precursor tolerance, 20 ppm; (2) MS/MS fragment tolerance, 0.25 Da; (3) maximal missed cleavages, one; and (4) variable modification, one (oxidation of methionine). Peptides were considered correct calls when the confidence interval was greater than 95%. To reduce redundancies in protein identification, data were processed further using ProteinCenter software (Proxeon).

Relative protein quantification by DeepQuanTR software

The DeepQuanTR software has been described in detail elsewhere (T.F., D.N., C.R., manuscript submitted). Briefly, after MS acquisition, data related to the individual peaks (fractions, intensities, m/z ratios) were loaded into the DeepQuanTR software, which performed a normalization of individual signal intensities to the internal standard peptides and an annotation (peptide identification and association with a parent protein). Normalized intensities for the individual peptides from all samples were used for the computation of DeepQuanTR peptide and protein scores, indicating the relative abundance of individual peptides and proteins in the various groups of samples.

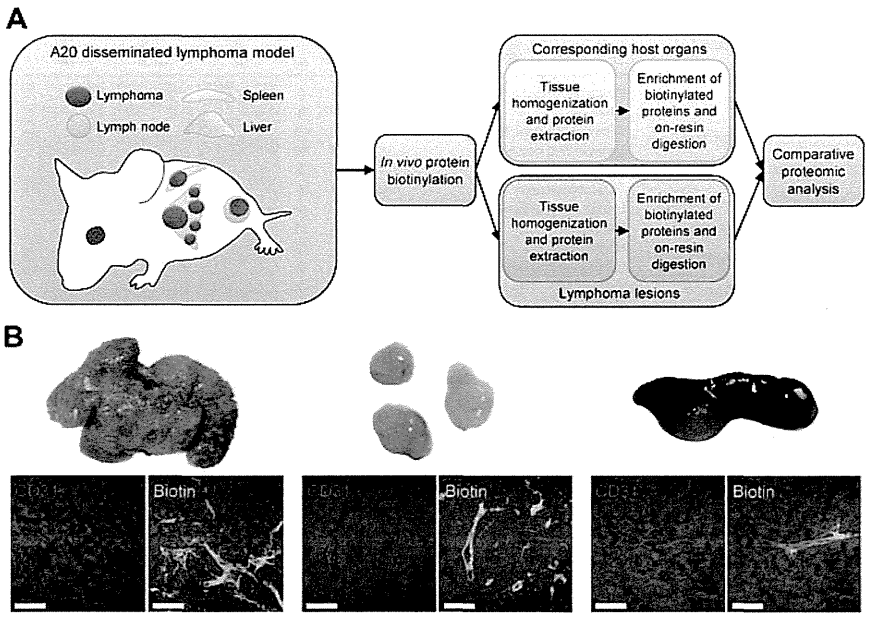

Figure 1. In vivo biotinylation of the bloodstream-accessible tissue compartment in a syngeneic mouse model of B-cell lymphoma. (A) Healthy and lymphoma-bearing mice were subjected to the terminal perfusion with a reactive ester derivative of biotin, leading to the covalent modification of proteins accessible from the bloodstream. Tumors and corresponding normal organs were excised and homogenized for the preparation of total protein extracts. Biotin-tagged proteins were enriched on streptavidin Sepharose, on-resin digested with trypsin, resulting peptides were separated by nanocapillary reverse-phase HPLC, and submitted to the comparative proteomic analysis. (B) Streptavidin-based detection of biotinylated structures (green) in perfused lymphoma tissues harvested from liver, lymph nodes, and spleen, in relation to vascular endothelium (CD31, red). Scale bars represent 50 μm.

Immunofluorescence analysis

Dual-color immunofluorescence was performed on 10-μm acetone-fixed cryostat sections. The following antibodies were used for immunostainings: rat anti–mouse activated leukocyte cell adhesion molecule (CD166), rat anti–mouse CD98, rat anti–mouse BST-2 (129c), and rat anti–mouse BST-2 (927) from eBioscience; rat anti–mouse endoglin, goat anti–mouse EMILIN-1, and rabbit anti–mouse PECAM-1 from Santa Cruz Biotechnology; rat anti–mouse transferrin receptor from Abcam; rat anti–mouse CD205 from AbD Serotec; goat anti–mouse clusterin from R&D Systems; rat anti–mouse PECAM-1 from BD Biosciences; and mouse anti–human BST-2 from Abnova. Appropriate Alexa Fluor 488– or 594–labeled secondary antibodies were purchased from Invitrogen. In vivo biotinylated structures were detected using Alexa Fluor 488–conjugated streptavidin (Invitrogen). Nuclei were counterstained with 4,6-diamidino-2-phenylindole (Invitrogen). All slides were examined on a LSM 510 Meta confocal laser scanning microscope (Carl Zeiss).

Analysis of in vivo targeting

To investigate target accessibility in vivo, BALB/c mice bearing disseminated or subcutaneous A20 lymphoma were intravenously injected with 50 μg of monoclonal rat IgGs (anti–BST-2 clones 927 and 129c and isotype control). Six hours after injection, tissues were excised, frozen in optimal cutting temperature (OCT), and stored at −80°C. In vivo injected monoclonal antibodies and ex vivo applied rabbit anti–mouse CD31 were detected using the secondary antibodies donkey anti–rat Alexa Fluor 488 and goat anti–rabbit Alexa Fluor 594. Sections were analyzed on a LSM 510 Meta confocal laser scanning microscope.

Therapy experiments

BALB/c mice were inoculated subcutaneously with 10^7 A20 cells to induce localized lymphoma tumors in the left flank. Five days after injection, when palpable tumor nodules have developed, mice were grouped (n = 5 per group) to maximize uniformity and injected with 5 mg/kg of the monoclonal anti–BST-2 antibody 927, 5 mg/kg of the monoclonal anti–BST-2 antibody 129c, or 5 mg/kg of an isotype control IgG (all antibodies were of the rat IgG2b isotype). Injections were performed once weekly for a total of 3 injections. Tumor volume was measured using a digital caliper and calculated according to the formula $L \times W^2 \times 0.5$ (L indicates length; and W, width).

Immunohistochemistry

Human lymphoma specimens were retrieved from consultation files of the Institute of Pathology, University Hospital Schleswig-Holstein, Kiel, Germany. Cryosections of 6-μm thickness were fixed in chilled acetone, rehydrated in Tris-buffered saline (50M Tris, 100mM NaCl, pH 7.4), and blocked with 20% fetal calf serum (Invitrogen). Mouse anti–human BST-2 antibody (Abnova) was detected using polyclonal rabbit anti–mouse IgG and the alkaline phosphatase–antialkaline phosphatase complex (Dako Denmark). Fast Red (Sigma-Aldrich) was used as phosphatase substrate, and slides were analyzed on an Axiovert S100 TV microscope (Carl Zeiss).

Statistical analysis

Differences in tumor growth among treatment groups were assessed using the Student *t* test. *P* values less than .05 were considered significant.

Results

In vivo protein biotinylation of disseminated B-cell lymphoma

Twelve lymphoma-bearing mice and 6 age-matched healthy BALB/c mice were subjected to a terminal perfusion procedure for the in vivo biotinylation of accessible proteins (Figure 1A). After anesthesia, the systemic circulation was perfused by intracardiac administration of an aqueous solution of Sulfo-NHS-LC-biotin (1 mg/mL, 10 mL) over 10 minutes at 100 mm Hg, followed by perfusion with quenching solution to block unreacted biotin ester. The efficient biotinylation of proteins in the most accessible structures (vascular endothelial cells, subendothelial extracellular matrix, and perivascular tumor and stroma cells) was confirmed using a streptavidin-based detection method (green fluorescent staining in Figure 1B), as illustrated by CD31 costaining (red) in lymphoma lesions from liver, lymph nodes, and spleen. After in vivo biotinylation, normal organs and lymphoma tissues were excised, homogenized in the presence of 2% SDS, and submitted to chromatography on streptavidin-Sepharose. After extensive washing, biotinylated proteins were tryptically digested on-resin. The resulting peptides were separated by reverse-phase nano-HPLC, mixed with constant amounts of 4 commercially available peptides

serving as internal standards for relative quantification, and analyzed by MALDI-TOF and MALDI-TOF/TOF mass spectrometry.

Bioinformatic processing of MS data

The DeepQuanTR software, which allows a pairwise comparison of the average normalized signal intensities for multiple tryptic peptides corresponding to the same protein in different tissue samples, was used to identify differentially expressed proteins in pairs of lymphoma lesions and their corresponding normal organs (hepatic lymphoma vs normal liver, nodal lymphoma vs normal lymph nodes, splenic lymphoma vs normal spleen). We identified 520 nonredundant proteins with 2 or more peptides in liver, 295 in lymph node, and 368 in spleen samples (supplemental Table 1, available on the *Blood* website; see the Supplemental Materials link at the top of the online article). Color-coded DeepQuanTR-computed expression values of all accessible proteins identified in lymphoma lesions grown in liver, lymph nodes, and spleen can be found as supplemental Figure 1. Proteins up-regulated in individual lymphoma samples compared with the average protein expression in the corresponding healthy host organ were coded in green, and down-regulated proteins were displayed in red. The color intensity relates to the magnitude of the differences in MS signal intensities (supplemental Figure 1).

Virtually all lymphoma-associated cell-surface antigens identified so far are also expressed on their nonmalignant counterparts as well.[15] Thus, we focused our attention on antigens that were consistently up-regulated at all anatomic lymphoma localizations. In this analysis, all proteins identified with 2 or more peptides in at least 1 of the 3 lymphoma localizations were included. A total of 271 proteins were identified in all 3 lymphoma-normal organ pairs; 58 of them were up-regulated more than 10-fold in hepatic, nodal, and splenic lymphoma lesions (corresponding to an average DeepQuanTR value > 2.30). A selection of differentially expressed candidates is presented in Figure 2. These proteins include ITI-HC3, transferrin receptor, fibulin-2, PK-120, leucyl-cystinyl aminopeptidase, bone marrow stromal antigen 2 (BST-2, CD317), activated leukocyte cell-adhesion molecule (CD166), EMILIN-1, basigin, elastin, tubulointerstitial nephritis antigen-like, clusterin, and CD98 heavy chain. Classic endothelial or extracellular matrix proteins previously known to be involved in tumor angiogenesis and/or proposed as targets for vascular targeting applications, such as endoglin (CD105), lactadherin, vitronectin, thrombospondin-1, fibronectin, tenascin-C, MECA-32, PECAM-1 (CD31), aminopeptidase N (CD13), CD36, and several collagens and integrins, were also identified (Figure 2; supplemental Table 1). Literature findings for proteins previously known to be expressed in lymphomas and/or during angiogenesis for a selection of the 58 proteins that were more than 10-fold up-regulated are presented in supplemental Table 2.

Validation of accessible lymphoma targets

To validate the DeepQuanTR findings, we focused our attention on a subset of candidate antigens for which antibodies suitable for immunofluorescence were available. Eight proteins were studied in detail by immunofluorescence analysis of the tumor/normal liver border, which confirmed the protein expression data derived from the DeepQuanTR analysis (Figure 3). Costaining with CD31 revealed a vascular pattern of staining for certain antigens, including novel (eg, BST-2) and previously known (eg, endoglin) markers of angiogenesis, as well as matrix components (eg, clusterin) or proteins expressed on the surface of tumor cells (eg, transferrin receptor, or CD98). Higher magnification confocal images of all candidate proteins in relation to CD31 staining are presented in supplemental Figure 2. Some of the proteins identified

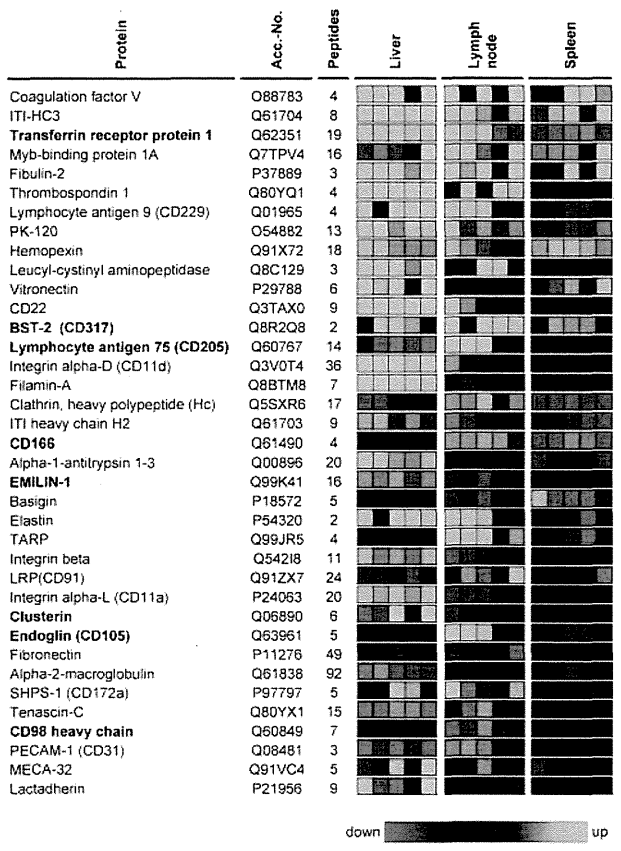

Figure 2. Selection of proteins overexpressed at all 3 lymphoma localizations. A selection of proteins that were consistently found up-regulated at nodal and extranodal lymphoma localizations is shown. Protein abundances in 5 lymphoma samples are displayed for each organ/lymphoma pair with a color code related to the corresponding DeepQuanTR score (maximum = e^6-fold up-regulation; minimum = e^6-fold down-regulation). Proteins up-regulated in comparison to the average protein expression in the corresponding normal host organ are displayed in green, down-regulated proteins in red. Proteins are sorted in descending order according to the average regulation score calculated from all 3 localizations. Antigens selected for further investigation are marked in bold.

appeared to be completely undetectable in adjacent normal liver tissue with a clear-cut margin of staining at the normal tissue/lymphoma border (eg, BST-2, clusterin, or EMILIN-1). Others displayed a considerable expression also in normal tissue, yet at a lower intensity compared with their expression in lymphoma lesions (eg, endoglin, CD98; Figure 3).

BST-2 as a novel marker of lymphoma blood vessels

BST-2 was one of the most interesting vascular markers of lymphoma identified in the chemical proteomic analysis. To the best of our knowledge, a vascular expression of the BST-2 protein in tumors had not been described before. In light of the excellent colocalization of BST-2 with the vascular marker CD31 in lymphoma blood vessels, while the antigen was completely undetectable in normal liver, we decided to further explore BST-2 as a potential lymphoma vascular target for antibody-based pharmacodelivery applications and therapy. First, we performed systematic immunofluorescence expression studies of normal mouse organs (Figure 4A). BST-2 (green) was virtually undetectable in the vasculature of all organs analyzed, including brain, heart, lung, liver, spleen, lymph nodes, kidney, intestine, kidney, and skeletal muscle, whereas CD31 (red) was always detectable in the same experimental setup. A distinct, albeit not vascular, expression of BST-2 was found in spleen and lymph nodes, consistent with its known expression in plasmacytoid dendritic cells.[23] Interestingly, expression of

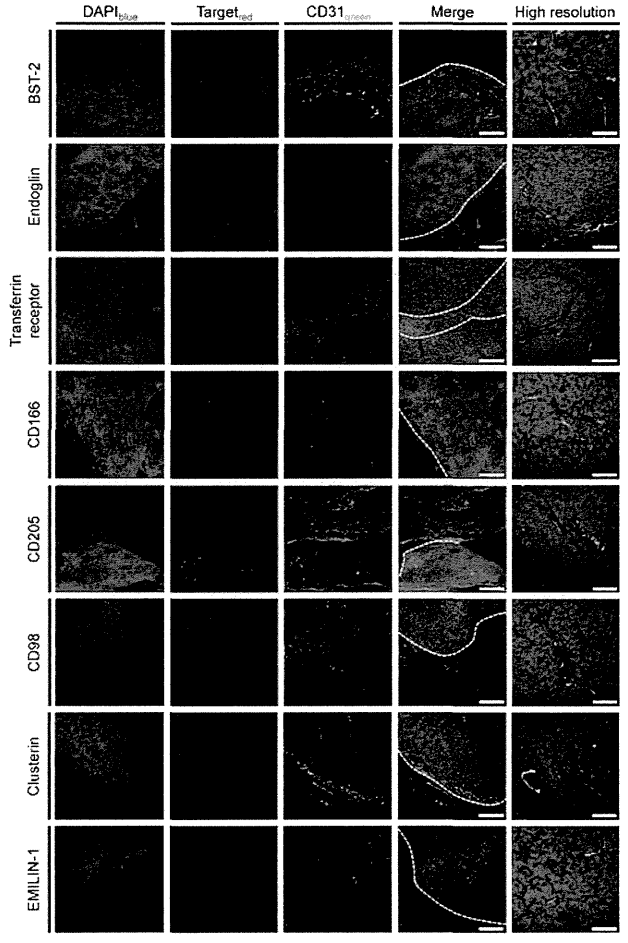

Figure 3. Validation of DeepQuanTR results. Immunostainings of the lymphoma/normal liver border (scale bars represent 200 μm) and with higher magnification of hepatic lymphoma lesions (scale bars represent 50 μm) using antibodies against 8 candidate antigens found to be up-regulated in the proteomic analyses are presented. Proteins of interest are shown in red, CD31 in green, and nuclei in blue. Lymphoma nodules are easily identified by a higher cellular density. Costaining with CD31 revealed that proteins from different localizations within the bloodstream-accessible tissue compartments (vascular endothelial cells, subendothelial matrix and stroma, perivascular tumor cells) have been modified by in vivo biotinylation and identified using DeepQuanTR. Dotted lines in merged images indicate the tumor/liver border. Slides were viewed with an LSM510 Meta confocal microscope (Carl Zeiss) using 10×/0.45 W and 40×/1.2 W water objectives and Fluorescent Mounting Medium (Dako). Images were acquired with the LSM510 Meta confocal laser scanning microscope and software provided by the manufacturer (Carl Zeiss). Images were manipulated using ImageJ software, Version 1.42q (available at http://rsb.info.nih.gov/ij/).

BST-2 could also be observed in the vasculature of subcutaneously implanted human lymphoma xenografts grown in immunodeficient mice, including Ramos, DoHH-2, and SU-DHL-4 (representing Burkitt, follicular, and diffuse large B-cell lymphomas, respectively), indicating that the expression of BST-2 in the vascular bed is apparently induced by the lymphoma environment (Figure 4A). The spatial distribution of BST-2 and CD31 expression within the lymphoma vasculature was further analyzed by confocal laser scanning microscopy, revealing a virtually complete superimposition of BST-2 and CD31 signals (Figure 4B). The pattern of BST-2 expression was recapitulated using a second monoclonal antibody specific to a different BST-2 epitope (clone 927; supplemental Figure 3).

Monoclonal anti–BST-2 antibodies home to lymphoma-associated neovasculature in vivo

Next, we investigated whether BST-2 overexpressed in angiogenic endothelium of lymphoma blood vessels could be targeted in vivo by intravenously administered antibodies. Six hours after injection of rat anti–mouse BST-2 antibodies into mice bearing disseminated A20 disease or subcutaneous A20 tumors, tumors were excised and analyzed for the presence of rat immunoglobulins, as indicated by green fluorescent staining in Figure 5A. Counterstaining with rabbit anti–mouse CD31 IgG (red) illustrated the colocalization of in vivo administered anti–BST-2 and ex vivo applied anti-CD31 antibodies in the majority of all lymphoma blood vessels (yellow color in merged images), both in hepatic lymphoma lesions and in subcutaneous tumors. Occasionally, single vessels or branches appeared to be BST-2$^-$ (hollow arrowhead, Figure 5A), a finding that is probably the result of a transient blood vessel occlusion in vivo, as virtually all CD31$^+$ vessels were found to be BST-2$^+$ in ex vivo staining procedures. A control IgG of irrelevant specificity did not accumulate in lymphoma tissues under identical conditions (Figure 5A), indicating that the observed homing to lymphoma-associated blood vessels was specific and antigen-dependent. Similarly, a second anti–BST-2 antibody exhibited an identical targeting performance (supplemental Figure 4)

Targeting BST-2 inhibits lymphoma growth

Having demonstrated that BST-2 can be successfully targeted in vivo, we performed therapy experiments in mice bearing subcutaneous lymphoma tumors, featuring 3 once-weekly intravenous administrations (5 mg/kg) of the 2 independent monoclonal antibodies directed against distinct BST-2 epitopes (clones 129c and 927). Both antibodies were significantly more potent in inhibiting lymphoma growth than equal amounts of nontargeting IgG and inhibited tumor growth by 44% (clone 129c; $P = .014$) and 48% (clone 927; $P = .008$), respectively (Figure 5B). Normal animal behavior and the absence of weight loss indicated that anti–BST-2 therapy was well tolerated (Figure 5C).

BST-2 is expressed in human lymphoma vasculature

Finally, we validated the expression of the human homolog of mouse BST-2 in specimens of human lymphoma by immunohistochemistry. In analogy to mouse lymphoma, BST-2 was detectable in the vasculature of multiple aggressive and indolent non-Hodgkin lymphoma subtypes, including diffuse large B-cell lymphoma, Burkitt lymphoma, mantle cell lymphoma, follicular lymphoma, and chronic lymphocytic leukemia (Figure 6A-E). In certain cases, tumor cells also were found to strongly express BST-2 in addition to vasculature, as illustrated in a Burkitt lymphoma specimen (Figure 6B). Again, BST-2 colocalized with the endothelial marker von Willebrand factor (Figure 6G-I).

Discussion

Using terminal perfusion of lymphoma-bearing mice and chemical proteomics procedures, we have established and characterized an atlas of proteins expressed in close association with the neovasculature of nodal and extranodal lymphoma lesion while being virtually undetectable in normal organs. Previously, the identification of markers of angiogenesis has mainly relied either by transcriptomic studies[24] or by proteomic profiling of physically separated endothelial plasma membranes.[25] In our study, from a total of 271 proteins that were simultaneously identified at all 3 lymphoma localizations, 58 showed an average DeepQuanTR protein expression value more than 2.30 (corresponding to a > 10-fold up-regulation compared with the normal organ), representing promising candidates for a detailed expression analysis. Some of these proteins have previously been described as

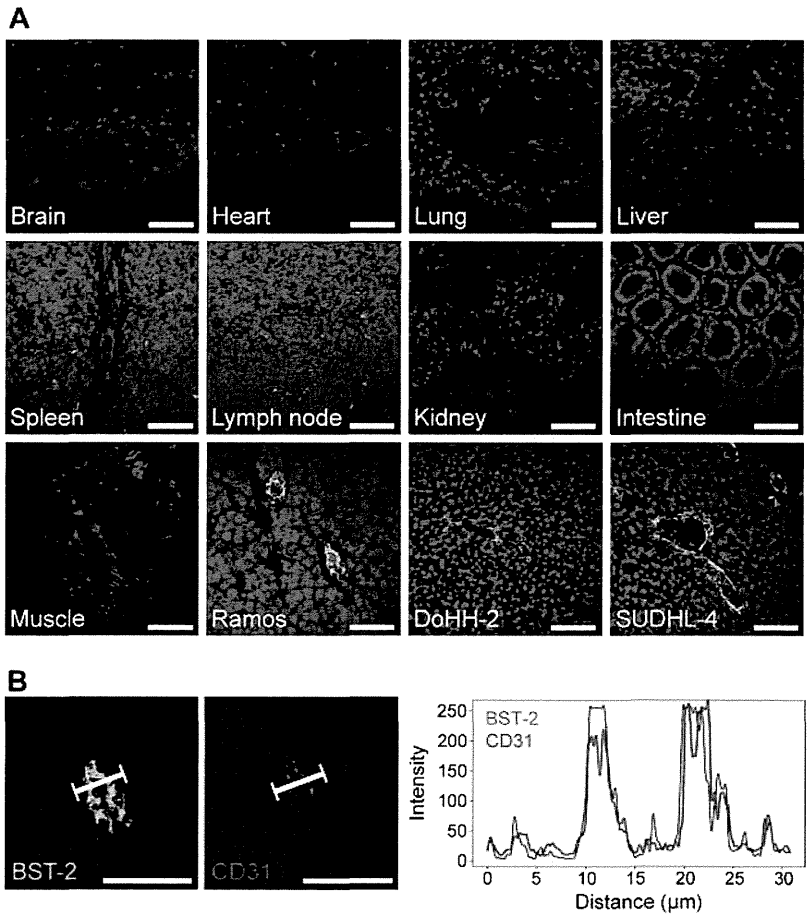

Figure 4. Expression of BST-2 in normal mouse organs and lymphoma xenografts. (A) Three-color confocal images of BST-2 staining (clone 129c, green), CD31 staining (red), and 4,6-diamidino-2-phenylindole counterstaining (blue) are shown. Although being undetectable in the vasculature of brain, heart, lung, liver, spleen, lymph nodes, kidney, intestine, and skeletal muscle, BST-2 was readily detectable in different lymphoma xenografts (Ramos, DoHH-2, SUDHL-4) in the same experiment, colocalizing to CD31 (yellow). As expected, a scattered cellular, but not vascular, expression of BST-2 was observed in lymphoid tissues. (B) Graphs displaying the spatial distribution of BST-2 and CD31 fluorescent signals in confocal microscopy were virtually superimposable. Scale bars represent 50 μm. Slides were viewed with an LSM510 Meta confocal microscope (Carl Zeiss) using 10×/0.45 W and 40×/1.2 W water objectives and Fluorescent Mounting Medium (Dako). Images were acquired with the LSM510 Meta confocal laser scanning microscope and software provided by the manufacturer (Carl Zeiss). Images were manipulated using ImageJ software, Version 1.42q (available at http://rsb.info.nih.gov/ij/).

either tumor up-regulated and/or expressed in tumor-associated neovasculature (supplemental Table 2). In accordance with previous observations, several serum components were found among the most differentially expressed proteins in neoplastic lesions (eg, complement C1q, coagulation factor V, complement factor B).[18] So far, it is not clear whether this observation results from the biotinylation of provisional tumor stroma that is known to contain blood coagulation products[26] or from the biotinylation of thrombotic events in tumor vasculature. Because of their abundance in blood, serum components were not further considered as candidate antigens for pharmacodelivery applications. In the future, the use of certain reactive derivatives of biotin with impaired extravasation properties (eg, charge, size) could potentially restrict the proteomic investigation to endothelial markers of lymphoma blood vessels.

The most interesting novel vascular marker of lymphoma identified in this study was BST-2 (also termed CD317, tetherin, or HM1.24). BST-2 was originally identified as a type II membrane glycoprotein with an unusual topology (one-pass transmembrane domain and C-terminal glycosylphosphatidylinositol anchor) that is preferentially overexpressed on multiple myeloma cells.[27,28] More recently, BST-2 has also been proposed as a tumor-associated antigen expressed in some solid tumor cell lines.[29-31] Furthermore, BST-2 has been found to block the release of enveloped particles (eg, HIV-1, Marburg virus, and Ebola virus) and may therefore be an important component of the antiviral innate immune defense.[32,33] This working hypothesis is supported by recent findings that HIV-1 viral protein U (Vpu) neutralizes the type I interferon up-regulated BST-2 expression by binding and thereby directing its β-TrCP2–dependent degradation.[34]

To our knowledge, expression of BST-2 in tumor vascular endothelium has not been described before. We did observe a scattered, albeit not vascular expression of BST-2 in normal lymphoid tissues, consistent with its known expression on mouse plasmacytoid dendritic cells.[23] Nevertheless, BST-2 was found to be up-regulated in lymphoma lesions developing in lymphoid organs in our proteomic analyses, possibly reflecting differences in accessibility of vascular endothelium and plasmacytoid dendritic cells and/or in absolute antigen abundance. Furthermore, BST-2 was detectable in blood vessels of indolent and aggressive non-Hodgkin lymphomas. In some cases, BST-2 was also strongly expressed by the lymphoma cells themselves, which can even be considered as an advantage for targeted pharmacodelivery strategies. Considering its restricted expression pattern targeting BST-2 with monoclonal antibodies or antibody derivatives might exert minimal unintended side effects. Indeed, therapy with 2 nonrelated monoclonal antibodies targeting distinct BST-2 epitopes significantly delayed lymphoma growth without apparent toxicities in mice. In principle, this antibody-induced tumor-growth delay could be explained either by antibody-dependent cell-mediated cytotoxicity (ADCC), complement-dependent cytotoxicity, or functional blocking (or a combination thereof). Indeed, antibodies of the rat IgG2b isotype have shown to be effective in promoting ADCC[35] and to eliminate disseminated human lymphoma in Scid mice.[36] However, the treatment of mice inoculated subcutaneously with human non-Hodgkin lymphoma B cells resulted in a minor tumor-growth reduction, even though murine macrophages were present in areas in these tumors that were depleted of tumor cells.[36] In humans, an ADCC-mediating monoclonal antibody to BST-2 has been reported to be well tolerated in phase 1 and 2 clinical trials in patients with multiple myeloma.[31]

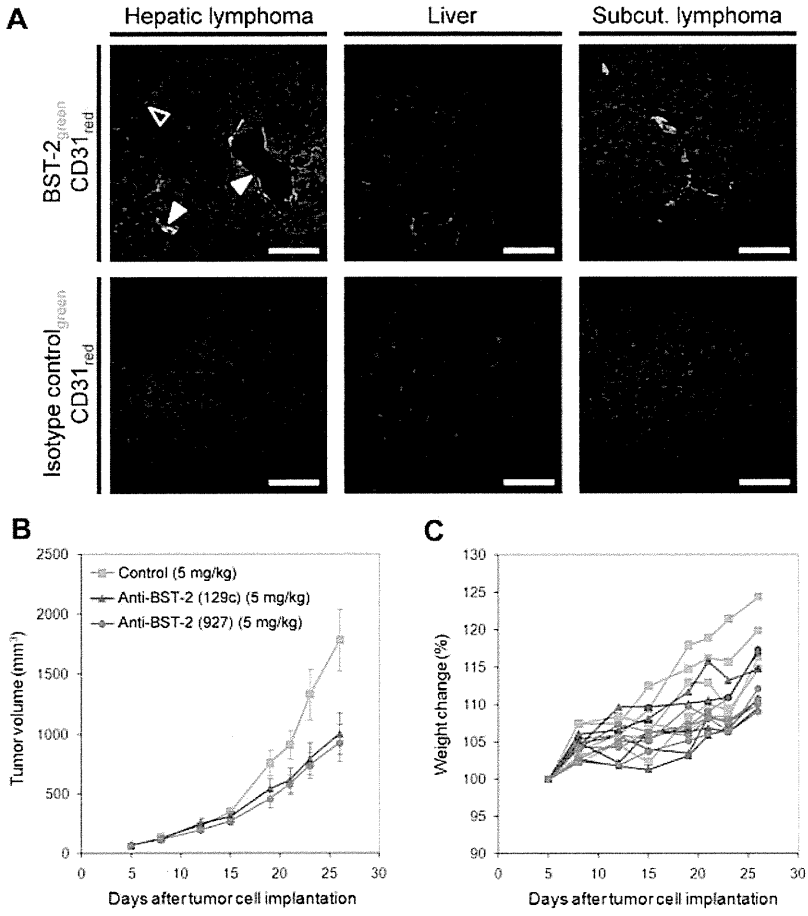

Figure 5. Monoclonal antibodies specific to BST-2 accumulate on lymphoma blood vessels and inhibit lymphoma growth in vivo. (A) A monoclonal rat anti–BST-2 antibody (clone 927) was intravenously injected into BALB/c mice bearing systemic or subcutaneous A20 lymphomas. Tumors and normal liver were excised 6 hours after injection, sectioned, and examined for the presence of rat IgG using donkey anti–rat Alexa Fluor 488 (green). Endothelial cells (CD31) were outlined in red. Although the anti–BST-2 antibody efficiently homed to lymphoma neovasculature in vivo (solid arrowheads), an isotype-matched control IgG did not accumulate on lymphoma blood vessels under identical experimental conditions. The hollow arrowhead indicates a BST-2–negative vessel that was most probably not perfused in vivo. Scale bars represent 50 μm. Slides were viewed with an LSM510 Meta confocal microscope (Carl Zeiss) using 10×/0.45 W and 40×/1.2 W water objectives and Fluorescent Mounting Medium (Dako). Images were acquired with the LSM510 Meta confocal laser scanning microscope and software provided by the manufacturer (Carl Zeiss). Images were manipulated using ImageJ software, Version 1.42q (available at http://rsb.info.nih.gov/ij/). (B) Tumor growth curves of A20 lymphomas subcutaneously implanted into BALB/c mice, treated with anti–BST-2 antibody 129c (5 mg/kg, 5 mice), anti–BST-2 antibody 927 (5 mg/kg, 5 mice), or isotype-matched control antibody (5 mg/kg, 4 mice). Treatment was administered intravenous once weekly for a period of 3 weeks. Both BST-2 antibodies significantly inhibited lymphoma growth ($P = .014$ and $P = .008$, respectively). (C) The lack of weight loss in each animal indicates that anti–BST-2 therapy was well tolerated.

The experience of our group with human monoclonal antibody derivatives, specific to alternatively spliced extracellular matrix components such as extra-domains of fibronectin and tenascin-C,[13,14,37-39] indicates that the neovasculature in solid tumors and in hematologic malignancies is quantitatively and qualitatively different, at the molecular level, from quiescent blood vessels in normal tissues. These properties can be exploited for the antibody-based delivery of therapeutic agents to the tumor neovasculature.[9-14] Indeed, immunocytokines and

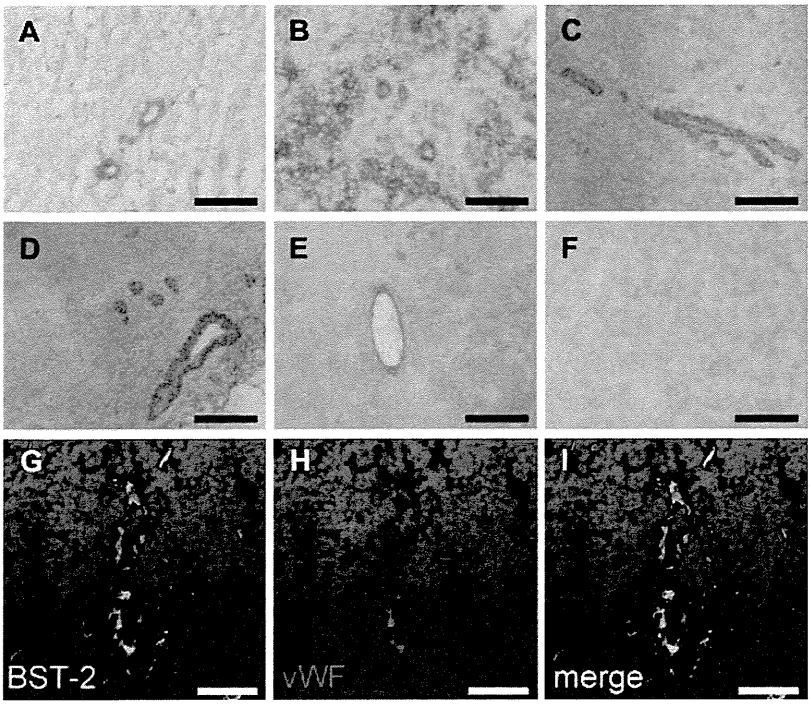

Figure 6. Expression of BST-2 in human non-Hodgkin lymphoma. BST-2 was detected in vascular structures of aggressive (A-C) and indolent (D-E) human non-Hodgkin lymphoma specimens using alkaline phosphatase–antialkaline phosphatase immunohistochemistry. Representative images of diffuse large B-cell lymphoma (A), Burkitt lymphoma (B), mantle cell lymphoma (C), follicular lymphoma (D), and chronic lymphocytic leukemia (E) are presented. Negative controls omitting the primary antibody were consistently negative (F). Although in most cases a predominant vascular staining was observed, also tumor cells were strongly immunostained in a case of Burkitt lymphoma (B). Slides were viewed with an Axiovert S100TV microscope (Carl Zeiss) using a 20×/0.40 Korr Ph2 objective and Glycergel Mounting Medium (Dako). Images were acquired using an AxioCam color camera and AxioVision software Version 4.7.1.0 (Carl Zeiss). Images were manipulated using ImageJ, Version 1.42q (available at http://rsb.info.nih.gov/ij/; A-F). Confocal images illustrate the colocalization of BST-2 and von Willebrand factor (vWF), exemplified on a section of chronic lymphocytic leukemia (G-I). Scale bars represent 100 μm (A-F) and 50 μm (G-I). Slides were viewed with an LSM510 Meta confocal microscope (Carl Zeiss) using 10×/0.45 W and 40×/1.2 W water objectives and Fluorescent Mounting Medium (Dako). Images were acquired with the LSM510 Meta confocal laser scanning microscope and software provided by the manufacturer (Carl Zeiss). Images were manipulated using ImageJ software, Version 1.42q (available at http://rsb.info.nih.gov/ij/; G-I).

radiolabeled antibodies specific to the EDA and EDB domain of fibronectin, and to the extra-domains A1 and D of tenascin-C are currently being investigated in clinical trials.[14,40] Similar pharmacodelivery strategies could be considered for derivatives of anti–BST-2 antibodies. In addition, the use of intact IgG products for the inhibition of lymphoma growth could be potentiated by suitable modifications of the immunoglobulin molecule, such as glycoengineering[41,42] or mutagenesis of the Fc antibody fragment.[43] In lymphoma, antibody-based pharmacodelivery strategies hold the promise to efficiently deliver therapeutic molecules to bulky tumor masses. It is tempting to speculate that bioactive agents (such as drugs with cleavable linkers or radionuclides) targeted to the bone marrow vascular compartment may exhibit therapeutic activity also in leukemia, given the fact that leukemic cells reside in close proximity to specialized vascular structures.[44]

The findings presented in this article could have considerable clinical relevance, considering that BST-2 is strongly expressed not only in the neovasculature of A20 lymphoma in mice, but also in blood vessels of human diffuse large B-cell lymphoma, Burkitt lymphoma, mantle cell lymphoma, follicular lymphoma, and chronic lymphocytic leukemia.

Acknowledgments

The authors thank the Functional Genomics Center Zurich for access to the HPLC and for technical support.

This work was supported by the Swiss National Science Foundation, the ETH Zürich, the European Union (ADAMANT and IMMUNO-PDT projects), the Swiss Cancer League, the SwissBridge Foundation, and the Stammbach Foundation. C.S. receives a bursary from the Deutsche Krebshilfe.

Authorship

Contribution: C.S. and C.R. designed the project, performed experiments, analyzed results, and wrote the manuscript; H.K. performed the proteomic analysis; B.B. performed perfusion experiments; T.F. designed the DeepQuanTR software and analyzed data; W.K. provided human lymphoma specimens; and D.N. designed the project, analyzed data, and wrote and reviewed the manuscript.

Conflict-of-interest disclosure: The authors declare no competing financial interests.

Correspondence: Dario Neri, Institute of Pharmaceutical Sciences, Department of Chemistry and Applied Biosciences, ETH Zurich, Wolfgang-Pauli-Strasse 10, CH-8093 Zurich, Switzerland; e-mail: neri@pharma.ethz.ch; or Christoph Roesli, Institute of Pharmaceutical Sciences, Department of Chemistry and Applied Biosciences, ETH Zurich, Wolfgang-Pauli-Strasse 10, CH-8093 Zurich, Switzerland; e-mail: christoph.roesli@pharma.ethz.ch.

References

1. Neri D, Bicknell R. Tumour vascular targeting. *Nat Rev Cancer.* 2005;5(6):436-446.
2. Schrama D, Reisfeld RA, Becker JC. Antibody targeted drugs as cancer therapeutics. *Nat Rev Drug Discov.* 2006;5(2):147-159.
3. Schliemann C, Neri D. Antibody-based targeting of the tumor vasculature. *Biochim Biophys Acta.* 2007;1776(2):175-192.
4. Carter PJ. Potent antibody therapeutics by design. *Nat Rev Immunol.* 2006;6(5):343-357.
5. Adams GP, Weiner LM. Monoclonal antibody therapy of cancer. *Nat Biotechnol.* 2005;23(9):1147-1157.
6. Thorpe PE. Vascular targeting agents as cancer therapeutics. *Clin Cancer Res.* 2004;10(2):415-427.
7. Dennis MS, Jin H, Dugger D, et al. Imaging tumors with an albumin-binding Fab, a novel tumor-targeting agent. *Cancer Res.* 2007;67(1):254-261.
8. Singh Jaggi J, Henke E, Seshan SV, et al. Selective alpha-particle mediated depletion of tumor vasculature with vascular normalization. *PLoS ONE.* 2007;2(3):e267.
9. Carnemolla B, Borsi L, Balza E, et al. Enhancement of the antitumor properties of interleukin-2 by its targeted delivery to the tumor blood vessel extracellular matrix. *Blood.* 2002;99(5):1659-1665.
10. Halin C, Rondini S, Nilsson F, et al. Enhancement of the antitumor activity of interleukin-12 by targeted delivery to neovasculature. *Nat Biotechnol.* 2002;20(3):264-269.
11. Borsi L, Balza E, Carnemolla B, et al. Selective targeted delivery of TNFα to tumor blood vessels. *Blood.* 2003;102(13):4384-4392.
12. Marlind J, Kaspar M, Trachsel E, et al. Antibody-mediated delivery of interleukin-2 to the stroma of breast cancer strongly enhances the potency of chemotherapy. *Clin Cancer Res.* 2008;14(20):6515-6524.
13. Schliemann C, Palumbo A, Zuberbuhler K, et al. Complete eradication of human B-cell lymphoma xenografts using rituximab in combination with the immunocytokine L19-IL2. *Blood.* 2009;113(10):2275-2283.
14. Sauer S, Erba PA, Petrini M, et al. Expression of the oncofetal ED-B-containing fibronectin isoform in hematologic tumors enables ED-B-targeted 131I-L19SIP radioimmunotherapy in Hodgkin lymphoma patients. *Blood.* 2009;113(10):2265-2274.
15. Cheson BD, Leonard JP. Monoclonal antibody therapy for B-cell non-Hodgkin's lymphoma. *N Engl J Med.* 2008;359(6):613-626.
16. Senter PD. Potent antibody drug conjugates for cancer therapy. *Curr Opin Chem Biol.* 2009;13(3):235-244.
17. Rizzieri DA, Akabani G, Zalutsky MR, et al. Phase 1 trial study of 131I-labeled chimeric 81C6 monoclonal antibody for the treatment of patients with non-Hodgkin lymphoma. *Blood.* 2004;104(3):642-648.
18. Rybak JN, Ettorre A, Kaissling B, Giavazzi R, Neri D, Elia G. In vivo protein biotinylation for identification of organ-specific antigens accessible from the vasculature. *Nat Methods.* 2005;2(4):291-298.
19. Roesli C, Neri D, Rybak JN. In vivo protein biotinylation and sample preparation for the proteomic identification of organ- and disease-specific antigens accessible from the vasculature. *Nat Protoc.* 2006;1(1):192-199.
20. Castronovo V, Waltregny D, Kischel P, et al. A chemical proteomics approach for the identification of accessible antigens expressed in human kidney cancer. *Mol Cell Proteomics.* 2006;5(11):2083-2091.
21. Scheurer SB, Rybak JN, Roesli C, et al. Identification and relative quantification of membrane proteins by surface biotinylation and two-dimensional peptide mapping. *Proteomics.* 2005;5(11):2718-2728.
22. Passineau MJ, Siegal GP, Everts M, et al. The natural history of a novel, systemic, disseminated model of syngeneic mouse B-cell lymphoma. *Leuk Lymphoma.* 2005;46(11):1627-1638.
23. Blasius AL, Giurisato E, Cella M, Schreiber RD, Shaw AS, Colonna M. Bone marrow stromal cell antigen 2 is a specific marker of type I IFN-producing cells in the naive mouse, but a promiscuous cell surface antigen following IFN stimulation. *J Immunol.* 2006;177(5):3260-3265.
24. St Croix B, Rago C, Velculescu V, et al. Genes expressed in human tumor endothelium. *Science.* 2000;289(5482):1197-1202.
25. Oh P, Li Y, Yu J, et al. Subtractive proteomic mapping of the endothelial surface in lung and solid tumours for tissue-specific therapy. *Nature.* 2004;429(6992):629-635.
26. Dvorak HF. Tumors: wounds that do not heal. Similarities between tumor stroma generation and wound healing. *N Engl J Med.* 1986;315(26):1650-1659.
27. Goto T, Kennel SJ, Abe M, et al. A novel membrane antigen selectively expressed on terminally differentiated human B cells. *Blood.* 1994;84(6):1922-1930.
28. Ohtomo T, Sugamata Y, Ozaki Y, et al. Molecular cloning and characterization of a surface antigen preferentially overexpressed on multiple myeloma cells. *Biochem Biophys Res Commun.* 1999;258(3):583-591.
29. Walter-Yohrling J, Cao X, Callahan M, et al. Identification of genes expressed in malignant cells that promote invasion. *Cancer Res.* 2003;63(24):8939-8947.
30. Wang W, Nishioka Y, Ozaki S, et al. HM1.24 (CD317) is a novel target against lung cancer for immunotherapy using anti-HM1.24 antibody. *Cancer Immunol Immunother.* 2009;58(6):967-976.
31. Kawai S, Azuma Y, Fujii E, et al. Interferon-alpha enhances CD317 expression and the antitumor activity of anti-CD317 monoclonal antibody in renal cell carcinoma xenograft models. *Cancer Sci.* 2008;99(12):2461-2466.
32. Jouvenet N, Neil SJ, Zhadina M, et al. Broad-spectrum inhibition of retroviral and filoviral particle release by tetherin. *J Virol.* 2009;83(4):1837-1844.

33. Neil SJ, Zang T, Bieniasz PD. Tetherin inhibits retrovirus release and is antagonized by HIV-1 Vpu. *Nature.* 2008;451(7177):425-430.
34. Mangeat B, Gers-Huber G, Lehmann M, Zufferey M, Luban J, Piguet V. HIV-1 Vpu neutralizes the antiviral factor Tetherin/BST-2 by binding it and directing its beta-TrCP2-dependent degradation. *PLoS Pathog.* 2009;5(9):e1000574.
35. Hale G, Clark M, Waldmann H. Therapeutic potential of rat monoclonal antibodies: isotype specificity of antibody-dependent cell-mediated cytotoxicity with human lymphocytes. *J Immunol.* 1985;134(5):3056-3061.
36. de Kroon JF, de Paus RA, Kluin-Nelemans HC, et al. Anti-CD45 and anti-CD52 (Campath) monoclonal antibodies effectively eliminate systematically disseminated human non-Hodgkin's lymphoma B cells in Scid mice. *Exp Hematol.* 1996; 24(8):919-926.
37. Kaspar M, Zardi L, Neri D. Fibronectin as target for tumor therapy. *Int J Cancer.* 2006;118(6): 1331-1339.
38. Brack SS, Silacci M, Birchler M, Neri D. Tumor-targeting properties of novel antibodies specific to the large isoform of tenascin-C. *Clin Cancer Res.* 2006;12(10):3200-3208.
39. Pedretti M, Soltermann A, Arni S, Weder W, Neri D, Hillinger S. Comparative immunohistochemistry of L19 and F16 in non-small cell lung cancer and mesothelioma: two human antibodies investigated in clinical trials in patients with cancer. *Lung Cancer.* 2009;64(1):28-33.
40. Santimaria M, Moscatelli G, Viale GL, et al. Immunoscintigraphic detection of the ED-B domain of fibronectin, a marker of angiogenesis, in patients with cancer. *Clin Cancer Res.* 2003;9(2): 571-579.
41. Ferrara C, Stuart F, Sondermann P, Brunker P, Umana P. The carbohydrate at FcgammaRIIIa Asn-162: an element required for high affinity binding to non-fucosylated IgG glycoforms. *J Biol Chem.* 2006;281(8):5032-5036.
42. Nimmerjahn F, Ravetch JV. Divergent immunoglobulin g subclass activity through selective Fc receptor binding. *Science.* 2005;310(5753):1510-1512.
43. Lazar GA, Dang W, Karki S, et al. Engineered antibody Fc variants with enhanced effector function. *Proc Natl Acad Sci U S A.* 2006;103(11): 4005-4010.
44. Sipkins DA, Wei X, Wu JW, et al. In vivo imaging of specialized bone marrow endothelial microdomains for tumour engraftment. *Nature.* 2005; 435(7044):969-973.

—Review—

抗体工学を駆使した創薬ターゲットの探索技術

鎌田春彦

Exploring Technique for Pharmaceutical Target Using Antibody Technology

Haruhiko Kamada

Laboratory of Biopharmaceutical Research, National Institute of Biomedical Innovation; 7-6-8 Saito-Asagi, Ibaraki, Osaka 567-0085, Japan.

(Received December 2, 2011)

A monoclonal antibody (Mab), due to its specific binding ability to a target protein, can potentially be one of the most useful tools for the functional analysis of proteins in recent proteomics-based research. However, the production of Mab is a very time-consuming and laborious process (*i.e.*, preparation of recombinant antigens, immunization of animals, preparation of hybridomas), making it the rate-limiting step in using Mabs in high-throughput proteomics research, which heavily relies on comprehensive and rapid methods. Therefore, there is a great demand for new methods to efficiently generate Mabs against a group of proteins identified by proteome analysis. Here, we describe a useful method called "Antibody proteomic technique" for the rapid generations of Mabs to pharmaceutical target, which were identified by proteomic analyses of disease samples (ex. tumor tissue, *etc.*). We also introduce another method to find profitable targets on vasculature, which is called "Vascular proteomic technique". Our results suggest that this method for the rapid generation of Mabs to proteins may be very useful in proteomics-based research as well as in clinical applications.

Key words——monoclonal antibody; proteomics; biomarker; biologics

1. はじめに

近年，ゲノム解析やジーンチップ解析などのオミクス研究の進展に伴い，バイオマーカー探索や創薬のための標的分子の探索が盛んに行われている.[1,2] このような医薬品開発に資する標的分子の探索は，画期的な医薬品を開発する上で最も重要なステップであり，探索の結果から得られた標的分子に作用する薬物は，これまで治療法のなかった疾患の治療に貢献すると考えられている．このような疾患の発症や悪化の原因となる標的分子の探索のうち，とりわけプロテオミクスを用いたタンパク質の発現解析は注目を集めており，医薬品の開発に貢献するものと期待されている.[3] しかしながら，上述したオミクス解析全般に言えることであるが，標的分子の探索から創薬ターゲットの発見につながった例はこれまでほとんどないのが現状である．疾患の発症や悪化に連動して発現変化が認められる疾患関連分子は，病態時に数百以上のオーダーで発現変動しており，そのほとんどが疾患の発症や悪化には直接関係していないものであるとされている.[4] したがって，画期的診断法・治療法を開発していくためには，このような疾患関連分子の中から，創薬に資する分子を効率よく同定する必要があり，これまで用いられてきた方法をより進歩させた新しい探索法の開発に期待が寄せられている．

このように標的分子を検出したり薬理効果発現を評価したりするためには，標的分子を認識可能なプローブが必要であり，標的分子候補タンパク質に結合活性を持つ抗体の開発がますます重要視されつつある．特に，最近では抗体そのものを医薬品化した抗体医薬品がリウマチやがんなど様々な難治性疾患に臨床応用され，バイオ医薬品の市場規模が急拡大している.[5] これまでに臨床応用された抗体医薬品としては抗サイトカイン抗体などの活性中和抗体や細胞表面のマーカー分子を認識する抗細胞抗体がほ

独立行政法人医薬基盤研究所バイオ創薬プロジェクト
(〒567-0085 大阪府茨木市彩都あさぎ7-6-8)
e-mail: kamada@nibio.go.jp

本総説は，日本薬学会第131年会シンポジウムS16で発表したものを中心に記述したものである．

とんどであるが，最近では受容体に結合して活性を示すアゴニスト抗体や2種類のマーカー分子を認識して活性を示すバイスペシフィック抗体なども臨床応用に向けた検討が進められつつある.[6]

このような抗体医薬は，従来の低分子医薬品や分子プローブでは困難な疾患に対する治療や診断が可能であるために，様々な難治性疾患の克服に向け大いに利用されつつあるところであるが，抗体医薬の開発を効率よく進めるためにはいくつかの問題点があることが知られている．その1つの問題点として，一般的に1種類の抗体の作製期間は，数ヵ月程度必要とされ，このことが原因となって標的分子が同定されてからその評価までには大きなタイムラグが生じており，タンパク質の中からスクリーニングする上での障害となっていることが指摘されている．

もし数多くの発現変動タンパク質に対する特異的抗体が一挙かつ迅速に作製できれば，定量解析（ELISA, Western blot（WB）, *etc.*），局在解析（免疫染色，WB, *etc.*），機能解析（細胞増殖活性，細胞分化解析，*etc.*）が可能になり，タンパク質の発現挙動と疾患の発症・悪化などとの連関解析が格段に進展するものと考えられる．そこでわれわれは，プロテオーム解析技術の最適化とともに，数多くの変動タンパク質の中から，創薬に向けて標的分子を絞り込む基盤技術の開発を行うために，プロテオミクスと抗体工学を融合させた新しい「抗体プロテオミクス技術」を開発した．本総説では，この「抗体プロテオミクス技術」を概説し創薬ターゲット候補分子の同定に至った例を示すとともに，抗体をバイオ医薬品として利用する際に有用な探索技術として「血管プロテオミクス」に関してもその研究成果を一部紹介する．

2. 抗体プロオミクス技術

抗体は生体内で外来異物由来のタンパク質抗原を認識し，それを捕捉するための生体防御分子としての役割を持っている．すなわち，あらゆる外来抗原に対して，結合可能なレパートリーを有するタンパク分子群である．その性質を利用し，古くからタンパク質の定性や定量のためのツールとして，生命科学の分野で活用されている．われわれは，この抗体の持つ性質に着目し，生体の抗体レパートリーを再現した抗体ライブラリを手に持つことで，抗原に結合可能な抗体分子を短時間で手に入れたいと考えた．この膨大な抗体ライブラリの中から目的の抗体を迅速に単離するための基盤技術としてわれわれはファージ抗体ライブラリに着目した．このファージ抗体ライブラリは，抗体の抗原認識部位にあたるV領域をリンカーで結んだ一本鎖抗体（scFV抗体）をファージの外殻タンパク質gⅢとの融合タンパク質としてファージ表面に提示しており，ファージウイルスの表面に提示させた一本鎖抗体をライブラリとして作製することが可能である.[7] この技術は，一般的に用いられるハイブリドーマ法とは異なり，*in vitro* のセレクションのみで迅速にモノクローナル抗体を単離することができ，2週間程度の短期間でモノクローナル抗体が得られる方法である．この技術を従来から知られる二次元電気泳動法などを利用したプロテオミクス技術と組み合わせ，単離・精製したタンパク質に対して上述した抗体ライブラリからの抗体の単離を行おうと考えた．さらに得られた抗体を利用し，免疫染色を利用した抗原の発現解析を組織マイクロアレイを用いて迅速に行うことにした．この組織マイクロアレイは，がんなどの疾患組織が直径1–2 mm程度の組織片として添付されたスライドガラスであり，一挙に100症例以上もの組織を免疫染色などで検出することが可能である.[8] この組織マイクロアレイを用いることで，これまで発現解析が困難であった組織を一挙に染色でき，極めて短時間にタンパク質の発現状態を知ることができる．この抗体ライブラリをプロテオミクス，さらに組織マイクロアレイと融合した「抗体プロテオミクス技術」をわれわれは独自に開発し，がんの標的分子の探索を行うことにした（Fig. 1）.[9]

まず，ナイーブファージ抗体ライブラリをウェスタンブロット等に用いられるメンブランに固相化した精製タンパク質に対してパンニングを行い，わずか10 ng程度のモデル抗原からでもモノクローナル抗体を得ることができた．さらに，この方法を乳がんの診断・治療に応用し，画期的な標的分子の探索を行うために，正常乳腺とのタンパク質比較解析を行った．その結果，十数種類前後の標的分子候補の中から最も有用な創薬ターゲットとしてEphrin Receptor A10（EphA10）と呼ばれる分子を同定した（Table 1）．この分子は，乳がん細胞に特異的に発現する上，既存の乳がんの標的分子として知られるHer-2よりも高い陽性率を示し，Her-2陰性患者